Design and Analysis of a micro-scale Heat Exchanger

Author

Ali Ammar Naqvi

Registration Number

00000170342

Supervisor

Dr. Emad Uddin

DEPARTMENT OF MECHANICAL ENGINEERING

SCHOOL OF MECHANICAL & MANUFACTURING ENGINEERING

NATIONAL UNIVERSITY OF SCIENCES AND TECHNOLOGY

ISLAMABAD

JUNE, 2020

Design and Analysis of a micro-scale Heat Exchanger

Author

Ali Ammar Naqvi

Registration Number

00000170342

A thesis submitted in partial fulfillment of the requirements for the degree of

MS Mechanical Engineering

Thesis Supervisor:

Dr. Emad Uddin

Thesis Supervisor's Signature: _____

DEPARTMENT OF MECHANICAL ENGINEERING

SCHOOL OF MECHANICAL & MANUFACTURING ENGINEERING

NATIONAL UNIVERSITY OF SCIENCES AND TECHNOLOGY,

ISLAMABAD

JUNE, 2020

Thesis Acceptance Certificate

It is certified that final copy of MS thesis written by Mr. Ali Ammar Naqvi (Registration No. 00000170342), of SMME has been vetted by the undersigned, found complete in all respects as per NUST statues/regulations, is free of plagiarism, errors and mistakes, and is accepted as partial fulfillment for award of MS degree. It is further certified that necessary amendments, as pointed out by GEC members of the scholar, have also been incorporated in this dissertation.

Signature: _____

Name of Supervisor: Dr. Emad Uddin

Date: _____

Signature (HoD): _____

Date: _____

Signature (Dean/Principal): _____

Date: _____

Th-4 Form

Declaration

I certify that this research work titled "*Design and Analysis of micro-scale heat Exchanger"* is my own work. The work has not been presented elsewhere for assessment. The material that has been used from other sources has been properly acknowledged/referred.

Signature of Student

Ali Ammar Naqvi

Master of Science in Mechanical Engineering

Plagiarism Certificate (Turnitin Report)

This thesis has been checked for Plagiarism. Turnitin report endorsed by Supervisor is attached.

Signature of Student
Ali Ammar Naqvi
Registration Number # 00000170342

Signature of Supervisor
Dr. Emad Uddin
Assistant Professor
School of Mechanical and Manufacturing Engineering
National University of Sciences and Technology
Islamabad, Pakistan

Copyright Statement

Acknowledgements

Firstly, I would like to acknowledge the support and guidance of my supervisor Dr. Emad Uddin, who listened to me with open ears, challenged me to explore new ideas and taught me the work ethic to conduct individual research. He has proven to be a very patient and considerate advisor.

I am thankful to Dr. Muhammad Sajid, Dr. Zaib Ali and Dr. Samiur Rahman Shah from among the faculty of Computational Mechanics research group for their constructive reviews, supportive comments and contributions to this work.

I would also like to thank my friends and family for their support, particularly my research fellows Muhammad Zia Ullah Khan and Wasim Anwar for their companionship and the many memorable moments along the way.

Finally, I owe a special debt of gratitude to my beloved parents for their unconditional love and support throughout my career.

Dedicated to my exceptional parents and adored siblings whose tremendous support and cooperation led me to this wonderful accomplishment.

Abstract

The effect of passive fluid mixing upon convective heat transfer across rectangular micro-channels within the laminar flow regime has been numerically investigated. Proposed model makes use of a novel diverging-converging base corrugation design combined with vortex generation methods. Resulting effect of passive fluid mixing upon convective heat transfer and hydrodynamic flow phenomena across rectangular micro-channels has been numerically investigated. The effect of increase in Reynolds number upon friction factor and Nusselt number was observed within the laminar flow regime. For this purpose, a combination of vortex generation in the upper region of flow and continuous flow disruption in the lower region was employed using optimized bends/connecting bridge and base corrugation respectively. Significant heat transfer enhancement was achieved through this combined effect. The subsequent work was verified for two independent case studies: 1) Bended-Corrugated channel, 2) Interacting-Corrugated channels. In the first case, an optimized bend generating Dean Vortices was combined with base corrugation, which provided flow disruption effect in the lower region of the channel. For high Reynolds numbers, the overall increase in Nusselt number of up to 32.69% and thermal performance enhancement of upto a maximum value of "1.285 TPF" was observed. For interacting channel model, a connecting bridge of varying width was introduced between adjacent channels for parallel and counter flow configurations, where only the counter flow configuration was found to generate counter rotating vortices. The said model in combination with base corrugation provided an improved performance reaching up to "1.25 TPF", however as opposed to bended channel, a major decrease in pressure drop of up to 26.88% was observed for this configuration. For both cases, the diverging-converging base corrugation was found to be dependent on width ratio as well as aspect ratio of the corrugation model. The experimentally determined relations for alumina nano-fluids provided by Rea and KKL models were compared for both cases and the Rea model was found to be geometry dependent as opposed to the generalized KKL model.

Key Words: *Passive mixing, Vortex generation, Interacting channels, Nano-fluids, Corrugation*

Table of Contents

List of Figures

List of Tables

Nomenclature

$\boldsymbol{Re}$	Reynolds number
$\boldsymbol{Nu}$	Nusselt number
$\boldsymbol{f}$	friction factor
$\boldsymbol{D_H}$	Hydraulic diameter (mm.)
$\boldsymbol{Aht}$	Base area of channel ($mm.^2$)
$\boldsymbol{Q}$	Total heat rate (J/s)
$\boldsymbol{\dot{m}}$	Mass flow rate (Kg/s)
$\boldsymbol{\dot{V}}$	Volume flow rate (m^3/s)
$\boldsymbol{h}$	Heat transfer co-efficient ($W/m^2.K$)
$\boldsymbol{v_{in}}$	Inlet velocity (m/s)
$\boldsymbol{P_{power}}$	Pumping power (W)
$\boldsymbol{Cp}$	Specific heat (J/Kg.K)
$\boldsymbol{\rho_f}$	Density of base-fluid (kg/m^3)
$\boldsymbol{\mu_f}$	Viscosity of base-fluid (Pa.s)
$\boldsymbol{k_f}$	Thermal conductivity of base-fluid (W/m.K)
$\boldsymbol{\rho_{nf}}$	Density of nano-fluid (kg/m^3)
$\boldsymbol{\mu_{nf}}$	Viscosity of nano-fluid (Pa.s)
$\boldsymbol{k_{nf}}$	Thermal conductivity of nano-fluid (W/m.K)
$\Delta\boldsymbol{T}$	Temperature difference (K)
$\Delta\boldsymbol{P}$	Pressure difference (Pa)

List of abbreviations

CFD	Computational Fluid Dynamics
MCHE	Micro-Heat Exchanger
SIMPLE	Semi Implicit Method for Pressure-Linked Equations
microns	micrometers
MEMS	Micro Electro-Mechanical Systems
FVM	Finite Volume Method

CHAPTER 1: INTRODUCTION

1.1 Background:

Homogeneity of wall temperature is an essential requirement for most industrial equipment as well as lab on chip devices. The recent advancements in microchip technology have provided immense functionalities within small sized equipment. Owing to their small size these micro-devices find their use in a large number of applications including the aerospace, biomedical, chemical, computing and automotive industry. However, the presence of large localized heat inside such devices greatly affects their performance and durability. This localized heat needs to be constantly removed for optimum performance. In this regard, micro-channel heat exchangers have come forth as an attractive solution to dissipate heat from small spaces. These heat exchangers are used as cooling devices with applications in small equipment like lab on chips as well as large scale equipment such as gas turbine blades and process industry. The easiest way to study such problems is through heat flux modeling where the heat generated by the component is used to predict the cooling load. In some cases, the heat flux generated by devices can be predicted with varying degrees of accuracy, however for most cases the variations in applications make it difficult for scholars to model the problem for practical scenarios where the flux cannot be predicted accurately. The highest allowable operating temperature of device is a parameter that is used to select appropriate heat sink. Since one of the primary objectives of micro-heat sinks under study is to maintain the temperature of equipment below a critical temperature, therefore their performance needs to be studied for cases where surface temperatures close to critical temperatures have already been achieved. In such extreme conditions, the resulting convective heat transfer performance of heat sink is of significant importance and can be used to determine the maximum heat dissipation ability. This in turn also provides the cooling effect of MCHE that can be achieved within the safe operational range of devices for different temperatures and flow rates.

1.2 Micro-channel Heat Exchangers:

The concept of small scale heat exchangers was first introduced by Tuckerman and Pease[1] at the Stanford University research lab in 1981. The MCHE are a class of heat

exchangers whose sizes are generally less than 1 mm. The operating fluid is forced to flow through confined spaces of channels with small hydraulic diameters. The working principles of these heat exchangers are the same as those of conventional heat exchange devices. Their small size allows them to be used for smaller applications and because of this intimate size they are widely used for cooling of electronic devices, however, in recent times this use has expanded to chemical, environmental as well as industrial applications. These devices have been classified by different scholars with small differences between each classification systems. Mehendale[2] referred to channels with cross sectional dimensions between 1 to 100 microns as micro-channels while channels of smaller dimensions were referred to as nano-scale channels. The Kandlikar [3] classification defines mirco-channels as those with smallest dimensions between 10 to 200 microns and side lengths bigger than these were referred to as mini-channels. The classification provided by Obot[4] has been adopted by many scholars [5]–[7], where the channels of hydraulic diameters of less than 1 mm. are referred to as micro-channels. These MCHE can also be classified on the basis of operating fluids, however in recent times the use of nano-fluids as coolants has become very popular and is the preferred coolant in comparison to others.

The MCHE provide a number of benefits in comparison to other forms of cooling. Due to their small size, they provide a higher surface to volume ratio and therefore require less coolant in comparison to conventional heat exchangers. The small volume of fluid flowing inside confined spaces provides more intimate contact of fluid with the cooling surface, thus achieving higher heat transfer rates. The operating fluid is forced across the small cross section of micro-channel and the resulting values of convective heat transfer co-efficient for flow across the length are studied. Where the heat transfer co-efficient is expressed in terms of thermal conductivity, hydraulic diameter and Nusselt number as will be discussed in the following chapters

1.3 Geometry

Forced convection through motion of fluid within confined spaces of sizes less than 1mm. are referred to as micro-channel heat exchangers. A number of geometrical variations within MCHE have been studied by different scholars. The cross sectional shape of micro-channels can be classified into different types with basic geometrical shapes as well as novel designs being encountered in this research area. Regular geometrical shapes such as circular,

triangular, rectangular, trapezoidal and elliptical geometries are commonly used as cross sections of these channels. These regular geometrical shapes can be further modified by applying corner of intermediate modifications to the geometry. The direction of fluid inlet can be axial, angular or perpendicular depending upon the applications, while along the length, the channels can be straight, spiral or curved as per design criteria defined by scholars.

1.4 Scope of Work

With the rapid development of MEMS (Micro Electro-Mechanical Systems), the use of lab on chip devices has become fairly common with applications in electronic chip cooling as well as chemical and biomedical applications. Polymerase chain reaction (PCR) is a common technique used to detect the presence of pathogens[8], [9] and hereditary disorders[10]. The entire testing process takes place in three successive steps of denaturation, annealing and extension, each of the station temperatures of 95, 55 and 72 °C respectively, needs to be maintained at constant levels for optimum performance. The work done by selva et al.[11], [12] required maintaining a certain temperature gradient, in order to control the motion of droplets and bubbles through thermo-capillary effect. The above mentioned examples underscore the importance of developing an efficient cooling system capable of maintaining constant surface temperatures of working areas.

The aim of the study was to observe the passive mixing and convective heat transfer enhancement for fluid flow across micro-channels. Base corrugation used in combination with vortex generation is a new concept introduced by the present study and no previous work has been done by scholars to study this combined phenomenon. Since the fluid problems can be modelled through numerical methods therefore the present work employs FVM based solution of Navier-Stokes equations to study the performance of novel MCHE design. The improved performance and design margins demand an optimized design and accurate prediction of flow. Nano-fluids are becoming increasingly common in such heat exchangers and the same have been employed as coolants during the course of this study. While the presented idea can be expanded to a number of areas, the current work has been limited to the study of below mentioned objectives.

1. Optimum aspect ratio for given short length micro-channel
2. Passive mixing using combined effect of vortex generation and base corrugation for two

novel design geometries.

a. Bended-Corrugated Single Channel Model:
    i. Optimum Bend Selection
    ii. Development of new corrugation model
    iii. Addition of commonly used Metal-oxide (Al_2O_3) nano-particles to DI water.
b. Interacting-Corrugated Dual Channels:
    i. Introduction of connecting bridge and bridge angle study for straight/bended channels
    ii. Parallel flow and Counter flow phenomena
    iii. Flow mixing phenomenon for geometric variations.
    iv. Base corrugation effect and nano-fluid study

CHAPTER 2: LITERATURE REVIEW

The origin of micro-channel heat sinks can be traced back to Tuckerman and Pease[1], who introduced this concept at Stanford University in 1981, by demonstrating the benefit of enhanced heat transfer in such devices. Due to their size, these devices provide a higher surface area contact for heat dissipation[13]. Knight et al.[14] formulated a solution scheme for both laminar and turbulent flow regimes in micro-channels. While working at micro-scale the capability of macro-scale theory to accurately predict micro-scale phenomenon is of significant interest. The transferability of these relations has been contested by a few researchers with a few contradictory results being brought forth[15], [16] . However, most scholars were unable to conclude major differences between macro and micro-scale applications. The experimental study of Mishan et al.[17] was based on heat transfer and pressure drop across channels. They concluded that the conventional theory holds good for prediction of flow in micro-channels. Xu et al[18] numerically studied the flow characteristics for Reynolds number between 20 to 4000 concluding that the flow in micro-channels was in agreement with theoretical navier stokes equations. Therefore the earlier reported discrepancies can be attributed to scaling effect and measurement uncertainties due to viscous heating, wall roughness, entrance effects and temperature dependent properties of fluids [19]–[21].

The above scaling effects were subsequently studied by a few scholars who determined the entrance length in micro-channels. Whenever the length of micro-channels is small, the channel entrance length cannot be ignored and needs to be addressed [3]. Ahmad and Hassan[22] experimentally studied the hydrodynamics of flow in the entrance region and developed an empirical relation independent of aspect ratio. Galvis et al.[23] studied the effect of hydraulic diameter and aspect ratios using numerical simulations. He proposed separate correlations for different range of aspect ratios and Reynolds number contradicting the earlier study irrespective of aspect ratios by Ahmad and Hassan[22].

Upadhye and Kandlikar et al.[24] studied the aspect ratio optimization for micro-channels against different boundary conditions. Gao et al.[25] studied water flow in silicon ducts of rectangular cross-section. Gamrat et al.[13] numerically studied the conduction and entrance region for laminar flow of water across rectangular channels. Their geometry was modelled against the experimental work of Gao et al.[15]. The numerically formulated Poiseuille number

values were found to be considerably smaller than the ones given developing flow equation by Shah and London[26] and the observed deviation was attributed to the entrance region effect. Dharaiya and Kandlikar[27] heat transfer in rectangular micro-channels for developing and fully developed flow cases, concluding that the Nusselt number decreases with increase in aspect ratio for one or two sides heated boundary conditions. Moharana and Khandekar[28] concluded that the average Nusselt number decreases with increasing aspect ratio until an aspect ratio value of "2" after which it starts increasing.

Peng and Peterson[29] experimentally investigated the heat transfer characteristics of water through micro-channels. It was found that the heat transfer in laminar regime is dependent on aspect ratio of the channel while small resistance values were recorded in case of turbulent flow comparison with classical relations. Sahar et al[30] studied the single and multi-channel configurations for different hydraulic diameters summarizing that the flow transition from laminar to turbulent regime occurs at Reynold number values beyond 1600. While Zhang et al.[31] experimentally determined the flow transition region range of Reynolds number between 1200-1600 for channels of hydraulic diameter between 0.48 to 0.84mm. The study by Harms et al.[21] concluded that the transition occurs at 1500 Re. Since the present study has been limited to laminar flow regime, therefore a range of $50 \leq Re \leq 1000$ has been identified as the operating range for accurate prediction of flow behavior within the laminar flow regime.

A three dimensional model for conjugate heat transfer was developed by Fedorov and Viskanta[32] who concluded that the thermo-physical properties are temperature dependent as uniformity in average wall temperatures was observed along the channel. Hetsroni et al.[33] studied hydrodynamic characteristics of laminar flow in micro-channels with heat flux boundary condition, wall conduction, energy dissipation and temperature dependent fluid properties of fluid. It can be concluded that for an accurate problem formulation the heat transfer should be three dimensional and fluid properties need to be to be temperature dependent.

Renksizbulut and Niazmand[34] studied the heat transfer characteristics within entrance region of trapezoidal channels for laminar flow and T boundary condition. The performance of thermally developing flow with H1 boundary conditions and rectangular cross section micro-channels was numerically studied by Lee and Garimella[35]. The changes in convective heat transfer rates against aspect ratio were studied in order to obtain correlations for average Nusselt

number. This study was further extended by Smith and Nochetto[36] who studied aspect ratios of up to 100 in order to obtain a relation that covers broader range of aspect ratios.

Different schemes of fluid mixing have been investigated by scholars with the two main types being active and passive mixing of fluid. The passive mixing can be achieved by subtle variations in geometry, design, surface roughness, curvature or obstructions. The hydrodynamic study of curved channels was performed by Dean[37], [38]. According to his study on circular pipes, the curvature induces a centrifugal effect on fluid flow thus producing imbalance in velocity gradient. This instability known as Dean instability leads to fluid recirculation across the curve. Sudrasan[39] and di carlo[40] demonstrated the useful effects of dean vortices along with fluid mixing.

Xu et al.[41] studied the effect of boundary layer re-development through experimental studies. They demonstrated the decrease in pressure drop and enhanced heat transfer that can be achieved from the shortened effective flow length of these micro-channels. Therefore, the dean vortices combined with continued flow disruption in the lower region of the channel can be a very effective method of enhancing heat transfer. The cooling effect in microchannels can also be increased by the use of nanofluids as cooling mediums with many studies favouring the use of metal oxides as nano particles inside base fluids[42]–[44]. The effect of this fluid mixing can be exaggerated by the presence of nano-particles introduced in deionized water. Through this method the nano-particles can effectively transfer heat not only through the natural Brownian motion but also through fluid mixing.

In the present work, the performance enhancement of micro-channels due to geometric variations resulting in passive mixing with nanofluids as coolants has been compared to the conventional straight channel design with deionized water as cooling fluid. The numerical simulations have been conducted against variations in geometry, nanofluid type, concentration and Reynolds numbers within the laminar flow regime. The results have been expressed in terms of thermal performance factor to study the overall thermal performance of these channels.

CHAPTER 3: NUMERICAL MODELS

Since the study was conducted for steady laminar flow across rectangular micro-channels of varying hydraulic diameters, therefore the flow and heat transfer characteristics were modelled through the use of continuity, energy and momentum equations. As the steady flow does not vary with time and therefore the solution for equilibrium state was obtained through discretization of above mentioned equations. The present study assumes that the operating fluid acts as a single phase Newtonian fluid with no body forces or viscous dissipation. The flow condition is that of a steady state laminar flow in three dimensional domain with no slip condition at the fluid-solid interface. The CFD equation utilized for the present study have been discussed in the following section.

3.1 Single phase equations:

3.1.1 Conservation of Mass:

The conservation of mass commonly known as the continuity equation can be expressed as

$$\frac{\partial \rho}{\partial t} + \nabla.(\rho \vec{v}) = S_m \tag{3.1}$$

This generalized form of this equation is valid for compressible as well as incompressible flows. In the given equation the gradient is given in terms of density "ρ" and time “t”. The vector "$\overrightarrow{v}$" represents inlet velocity while the term "S_m" represents the external mass added to the system through inlet.

3.1.2 Conservation of Momentum:

The momentum conservation equation in an inertial frame of reference can be expressed as

$$\frac{\partial (\rho \vec{v})}{\partial t} + \nabla.(\rho \vec{v} \vec{v}) = -\nabla p + \nabla.(\vec{\tau}) + \rho \vec{g} + \vec{F} \tag{3.2}$$

$$\vec{\tau} = \mu \times \left\{ (\nabla \vec{v} + \nabla \vec{v}^T) - \frac{2}{3} \nabla . \vec{v} I \right\} \tag{3.3}$$

Where $\vec{\tau}$ is the stress tensor whose relation given by equation no. 3.3, the product of density and gravitational constant is the body force, while $\vec{F}$ is the external body force, I is the unit tensor, $\nabla\vec{v}^{T}$ is the volume dilation effect and "p" is the static pressure term.

3.1.3 Energy:

The energy equation can be expressed as

$$\frac{\partial}{\partial t}(\rho E) + \nabla.\left(\vec{v}(\rho E + p)\right) = \nabla.\left(k_{eff}\nabla T - \sum_j h_j \vec{J}_j + \left(\vec{\tau}_{eff}.\vec{v}\right)\right) + S_h \tag{3.4}$$

$$E = h - \frac{p}{\rho} + \frac{v^2}{2} \tag{3.5}$$

For the above mentioned equations, the term $\vec{J}_j$ represents the diffusion flux, while $k_{eff.}$ represents the effective thermal conductivity when a turbulent flow model is used. The three terms, enclosed in parenthesis, on right side of the equation no. 3.4 are the conduction, diffusion and viscous dissipation terms respectively, while the fourth term accounts for heat sources occurring either due to any chemical reaction or through any other external volumetric source.

CHAPTER 4: METHODOLOGY

Fluid problems are usually addressed through numerical, experimental or a combination of both techniques. The present numerical study of micro-channels focuses on a three dimensional conjugate heat transfer formulation. The operating fluids is de-ionized water with temperature dependent thermo-physical properties, while the solid material is copper having fixed thermo-physical properties, whose properties have been taken from the NIST database.

The entrance length is longer for laminar flow as compared to turbulent flows, this is due to the delayed flow profile development occurring as a result of shear forces at the boundary layer. Since the heat transfer rates are superior inside the entrance region, therefore it is favorable to delay the boundary layer formation, in order to achieve improved heat transfer rates. Passive mixing can be employed as a viable solution, however the design of channel should be capable of promoting heat transfer and mixing along the entire cross section and should not be limited to the boundaries of the channel, as was observed in literature. The flow cross section for the present case has been broken down into two parts with the corrugated model at the base of channel maximizing the conjugate heat transfer within the fluid in contact with the heating surface. The vortex phenomenon in the upper region of channel promoting homogeneity of temperature by distributing this heat evenly across the entire cross-section of fluid thus delivering an increased cooling effect and extracting maximum heat from the die surface.

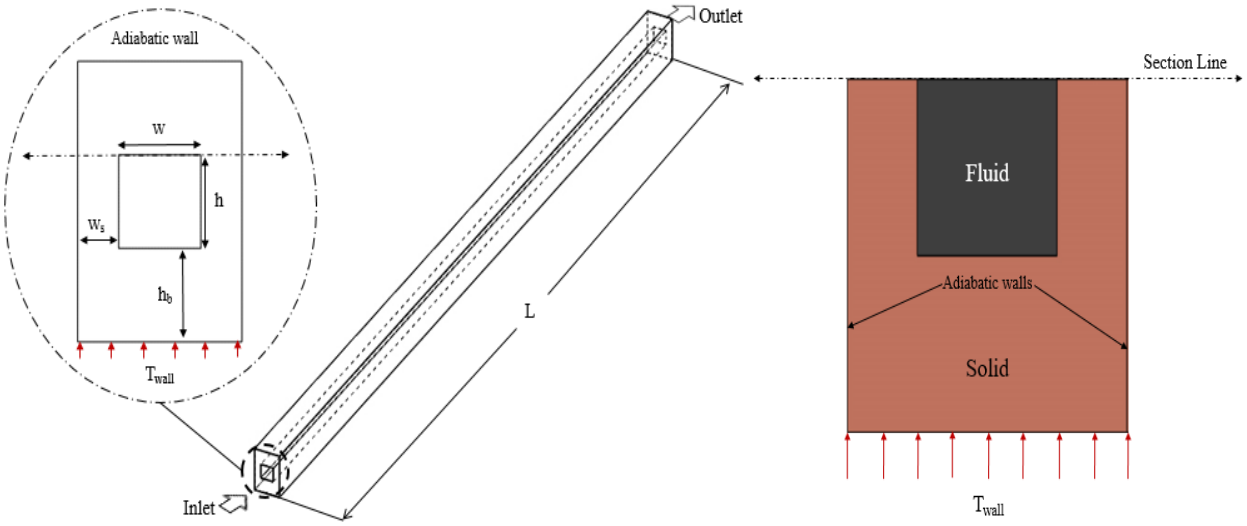

Fig. 1: a) Schematic of straight channel setup, **b)** Front view (Section) for domain definition

In this regard, different aspect ratios and hydraulic diameters of straight rectangular copper micro-channels, as shown in **Fig. 1Error! Reference source not found.-a**, were studied o determine the best performing geometry. The three dimensional problem setup is shown in **Fig. 1-b**, where the total length of channel was kept fixed at 18mm. since the lab on chip for which the solution is being developed is a square geometry with an equivalent side length. The analyses were performed for three different source temperatures to ensure continuity of performance pattern as shown in **Table 1**. The results were evaluated in terms of parameters such as Nusselt number and pressure drop. The dimensionless parameter of friction factor has been used as reference for comparison of pressure drop across different channels. The performance of finalized straight channel was enhanced though two separate design variations that have been numerically investigated to determine the effect of passive mixing.

Table 1: Straight Channel Parameters

S. No.	Width "w" (µm)	Height "h" (µm)	Length "L" (mm.)	Reynolds Number	Temperature (K)
1	50-350	50-350	18	100-1000	323.15
2					343.15
3					363.15

Details of parameters utilized for this study are given in **Table 1**. A symmetry condition was applied across the channel length splitting the domain into two halves about a vertical axis from the center. The simulation results were evaluated in terms of dimensionless parameters of Nusselt number and friction factor. The performance of finalized straight channel was enhanced though two separate design variations that were numerically investigated to determine the effect of passive mixing, as discussed in the following section.

4.1 Geometry

4.1.1 Bended-Corrugated Channel Model:

Un-interrupted flow mixing across bended-corrugated channels of fixed length was studied with incremental design evaluation steps. The heat transfer enhancement of best performing straight channel geometry was achieved through introduction of a series of two consecutive bends. Sharp cornered bends of different angles, as shown in **Fig. 2**, were introduced

along the length of the channel in order to determine the effect of sharp bends and the resulting fluid mixing effect. A mathematical model describing the relation of bend angle "***θ***" as a continuous variable was subsequently developed for both Nusselt number and friction factor parameters. The selection of optimum bend was carried out through response optimization of the aforementioned parameters. Since, sharp bends are not desirable from a design viewpoint, therefore the flow across bended geometry was mimicked through smoothing of sharp edges to obtain an equivalent curved channel model providing near identical performance. A new diverging-converging base corrugation scheme in the form of array was introduced at the bottom of the channel to promote flow disruption close to conjugate heat transfer phenomenon at the base. The corrugation model was studied for variation in width ratio as well as aspect ratio to determine the effect of change in these parameters over the corrugation scheme for the design. The bended channel with corrugation used for this study is given in **Fig. 2** while its dimensional parameters are given in **Table 2**. The base corrugation in this model has been used in the form of a series of diverging-converging pattern and resulting effects of flow disruption has been studied.

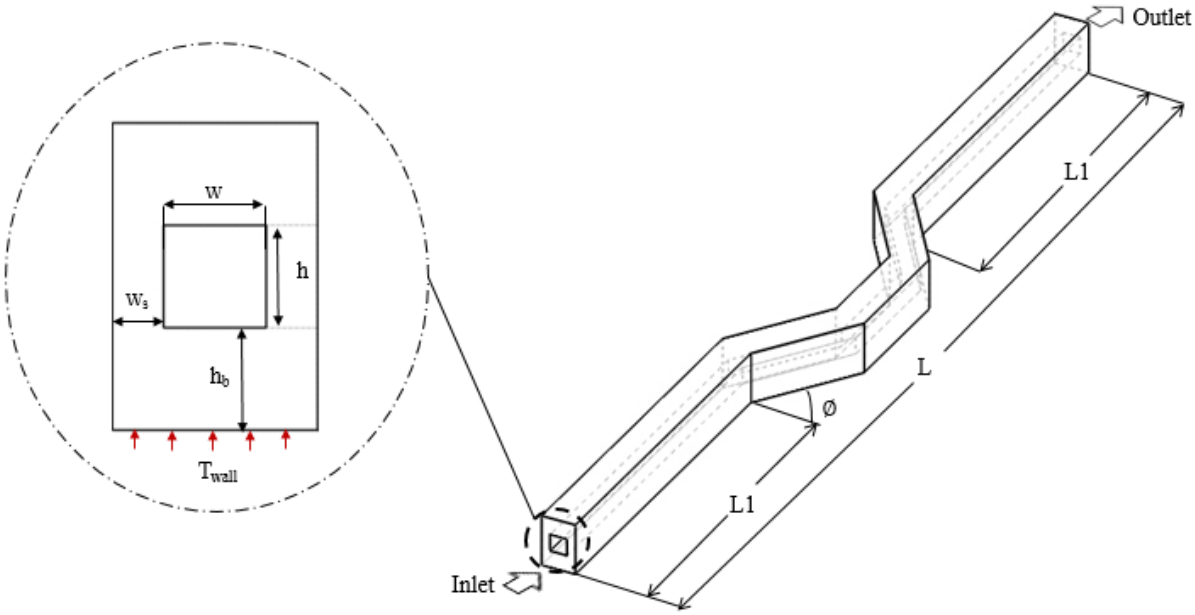

Fig. 2: Schematic of Bended Channel Geometry

A new diverging-converging base corrugation scheme as shown in **Fig. 3**, in the form of array was introduced to promote flow disruption close to conjugate heat transfer phenomenon at the base. The $W_{min.}$ and $W_{max.}$ As shown in the reference represent the minimum and maximum width respectively.

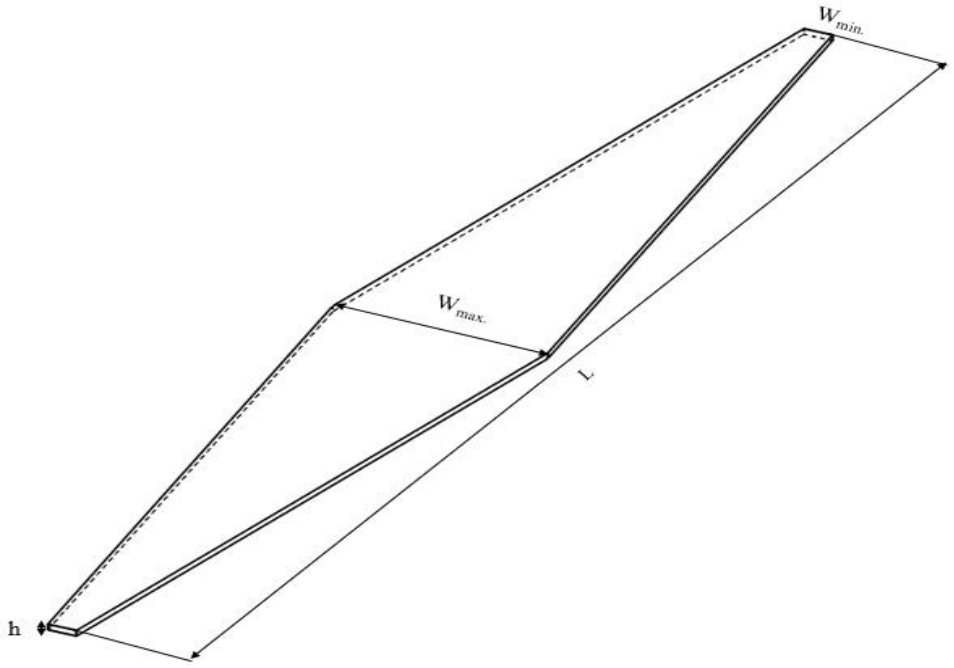

Fig. 3: Diverging-Converging corrugation geometry

The base corrugation scheme has been used in the form of a series of diverging-converging pattern and resulting effects of flow disruption have been studied. After finalization of optimized geometry, the effect of variation in operating fluid by adding nano-particles to de-ionized water was studied for the most efficient model.

Table 2: Single channel model parameters

S. No.	Symbol	Dimensions
1	L	60w
2	L1	20w
3	θ (deg.)	Ø -90°
4	W (μm)	300
5	H	w

4.1.2 Interacting-Corrugated Channel Model:

In case of interrupted flow mixing across micro-channels, an interacting channel design with connecting bridges of varying width close to both ends of the channel were introduced between two adjacent straight channels. The resulting fluid mixing phenomenon and heat transfer rates were studied for the interacting channel case. The numerical models were simulated for both parallel flow and counter flow cases. The three dimensional model of this geometry and its parameters are given in **Fig. 4** and **Table 3** respectively. The flow phenomenon

shows behavior of fluid across the bridge, with the counter flow model generating counter rotating vortices and providing superior performance for the same operating fluid and Reynolds numbers. The counter flow model was further investigated with varying dimensions of bridge width to determine the most effective design for fluid mixing. The model was then subsequently studied in combination with base corrugation scheme and variation in operating fluid. The final results for both cases were expressed in terms of thermal performance factor.

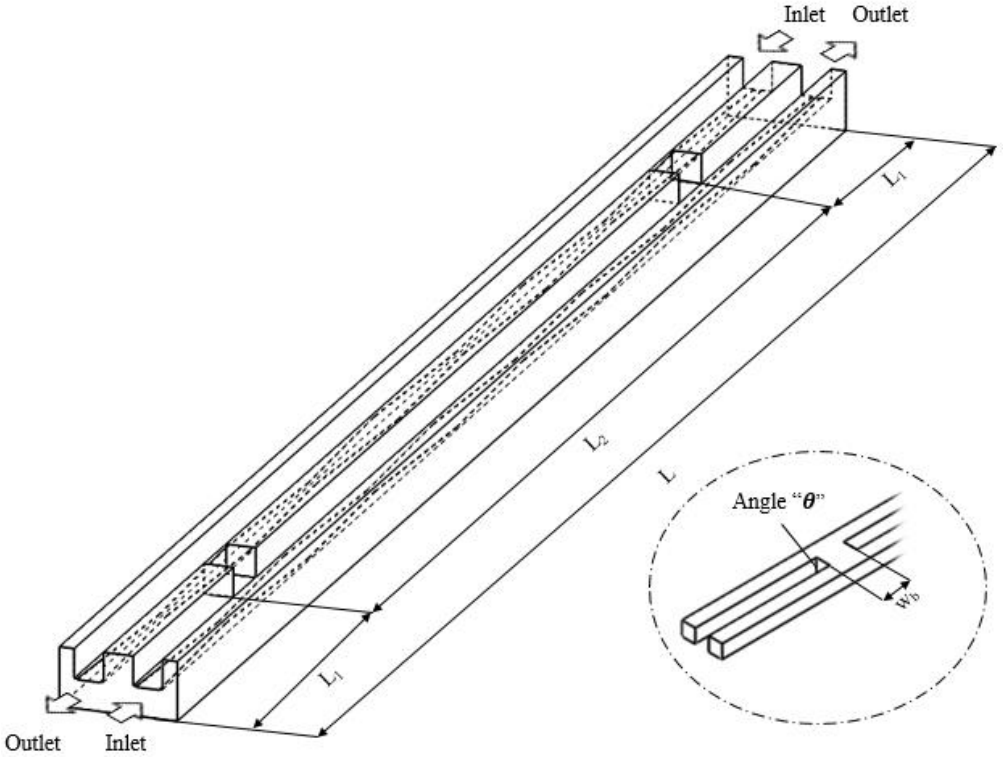

Fig. 4: Interacting-Corrugated channel geometry (counter flow)

Table 3: Interacting channel model parameters

S. No.	Symbol	Dimensions
1	L	60w
2	L1	10w
3	L2	40w
4	θ (deg.)	90°
5	W (μm)	300
6	H	W
7	S	W

4.1.3 Operating fluids:

The numerical study was conducted for two different types of coolants. De-ionized water with temperature dependent thermo-physical properties was utilized as the primary operating fluid for all simulations. For data reduction purpose, operating fluid was kept the same during design exploration of different geometrical schemes. The heat transfer enhancement study for geometries was conducted using de-ionized water as the coolant and the same DI-water was utilized as base fluid while formulating nano-fluids. The nano-fluids were studied for a combination of efficiency and economy. In this regard, different volume fractions of alumina nano-particles were added to the base operating fluid using the relations provided by Rea et al. [45]and KKL model[46]. Both of the previously discussed models were subsequently simulated for de-ionized water and nano-fluids to determine the difference in heat transfer rates of nano-fluids across straight channels against geometries that promote more mixing of flow across the channel. The properties of de-ionized water, alumina and copper have been given in **Table 4**, where the solid copper and alumina nano-particle properties have been obtained from NIST data.

Table 4: Properties of DI water and Copper

S. No.	Units	**De-ionized water** [47], [48]	Copper	Alumina
1	μ (Pa.s)	$0.0194 - 1.065 \times 10^{-4}T + 1.489 \times 10^{-7}T^2$	-	-
2	k (W/m.k)	$-0.829 + 0.0079T - 1.04 \times 10^{-5}T^2$	387.6	36
3	C_p (J/kg.k)	$5348 - 7.42T + 1.17 \times 10^{-2}T^2$	381	765
4	ρ (Kg/m^3)	998.2	8978	3970

4.1.4 Data reduction:

Optimum design point criterion was employed for data reduction purpose. The best design point of each aspect ratio was determined through response optimization between the dimensionless heat transfer and pressure drop parameters. While the selection of design point was based on optimization of parameters using the highest Nusselt number and lowest value of dimensionless pressure drop as desirable conditions, the basic idea behind this criterion can also be expressed in graphical form as shown in **Error! Reference source not found.**, which shows he utilization of trade-off between parameters and the resulting optimized Reynolds number selection for given geometry. Therefore, each of these design points were used as the reference performance evaluation points for their respective geometries. The initial straight channel simulations were performed for three separate critical temperatures, as shown in **Table 1** of the

previous section, however since a similar trend in all three temperatures was observed and varying heating temperatures showed no difference in graphical trends, therefore the lowest temperature was chosen as the design evaluation reference. Through above mentioned data reduction methods the total data was reduced from 1470 to 147 design points for considerations. The optimized design points for each geometry were then plotted against the dimensional elements to determine the best performing geometry. The subsequent geometrical analyses were carried out in terms of deionized water and only the finalized geometries were used for comparison between performances of different nano-fluids.

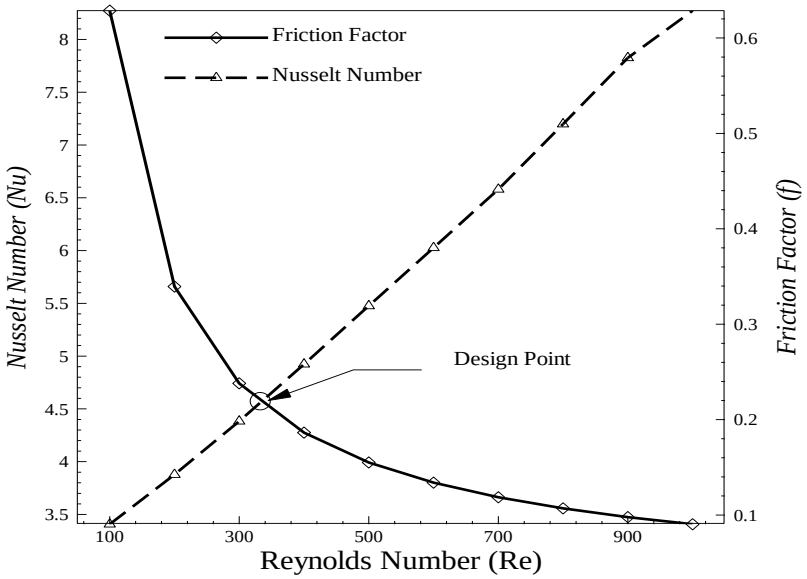

Fig. 5: Design Point

4.2 Assumptions:

The numerical model developed for this heat transfer problem was assumed to satisfy the following criteria:

1. Fluid incompressibility in three dimensional domain
2. Steady state laminar flow regime and heat transfer
3. Negligible radiation heat transfer and viscous heating
4. No-slip condition at the walls
5. No effect of channel surface roughness

4.3 Governing Equations:

Based on the above mentioned assumptions the governing equations for the given case can be expressed in the following form:

Conservation of Mass $$\nabla.(\rho \boldsymbol{V}) = \mathbf{0} \quad (1)$$

Where $\boldsymbol{V}$ is the velocity vector given as $\boldsymbol{V} = u\hat{\boldsymbol{\imath}} + v\hat{\boldsymbol{\jmath}} + w\hat{\boldsymbol{k}}$

Conservation of Momentum $$\boldsymbol{V}.\nabla(\rho \boldsymbol{V}) = -\nabla p + \nabla.(\mu \nabla \boldsymbol{V}) \quad (2)$$

Conservation of Energy (Fluid) $$\boldsymbol{V}.\nabla\left(\rho C_p T_f\right) = \nabla.(K_f \nabla T_f) \quad (3)$$

Conservation of Energy (Solid) $$\nabla.(k_s \nabla T_s) = \mathbf{0} \quad (4)$$

4.4 Boundary Conditions:

The boundary conditions imposed on the numerical model for this conjugate heat transfer problem are discussed as follows:

- Velocity inlet magnitude was determined against the specified Reynolds number using analytical relation. In the present case, the inlet velocity is a function of hydraulic diameter and Reynolds number between a given range 100≤ Re ≤1000. The ambient fluid inlet temperature is kept fixed at 298.15 K (25°C) and the values for temperature dependent properties can be found using **Table 4**.
- The solid-liquid interface was set to no-slip boundary condition.
- Dirichlet Boundary Condition known as "T" Boundary condition (Shah & London – 1978) where all the side walls have a fixed temperature.
- Pressure Outlet (inlet/outlet axial direction)

Since the principal flow is along the direction of z-axis, therefore the above mentioned data can be expressed as

Inlet: at z = 0, velocity inlet, $w = U_{in}, u = v = 0, T = T_{in}$

Outlet: at z = L, pressure outlet, $P = P_{\infty}$

Bottom Wall: Dirichlet boundary with constant temperature $T = T_s$

Side Walls: Adiabatic with constant temperature condition $T = T_w = T_{in}$

Inner walls: No slip condition, $u_s = v_s = w_s = 0$

The analyses were performed using "T" boundary condition for three critical base temperatures as already discussed in the previous section. The solid base is made of copper with de-ionized water as operating fluid having temperature dependent properties, flowing through copper ducts of rectangular cross section. The properties of both solid and fluid have been discussed in **Table 4**.

4.5 Solution Scheme:

The convergence for numerical solution of governing equations was achieved through ANSYS 18.1 - Fluent Module. The properties of fluid were expressed as piecewise second order polynomial functions in terms of Temperature variable. SIMPLE (Semi-implicit pressure linked equation) algorithm using second order upwind discretization was used to obtain the solution of governing equations. The details of solution scheme are given in **Table 5**. An absolute value of "1 x 10^{-5}" was chosen as the convergence criteria. The simulations were performed with double precision and the number of mesh elements for an average simulation were 4.32 million and 6.5 million elements for single and dual channel models respectively. The study was performed utilizing intel two Xeon X5660 processors, 12 cores with 64 gigabytes of RAM. The average computational time for a single channel case was four hours, while for dual channel model the average solution convergence time was six hours.

Table 5: Solution scheme for numerical simulations

S. No.	Discretization variable	Solution scheme
1	Pressure	Standard
2	Pressure-Velocity Coupling	SIMPLE
3	Momentum	Second order (upwind)
4	Energy	Second order (upwind)

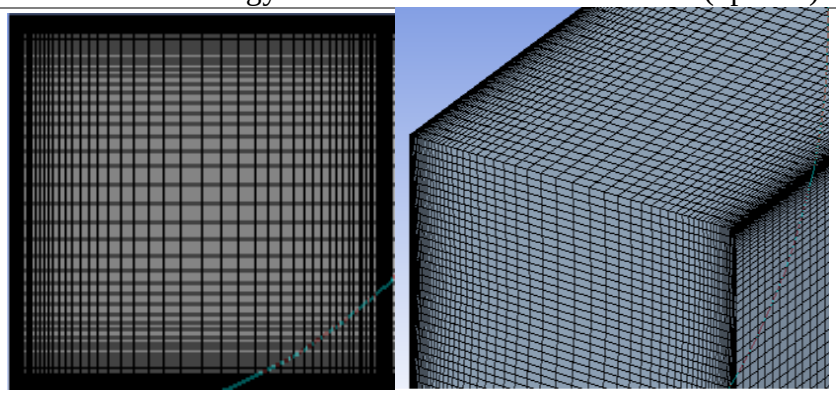

Fig. 6: Mesh cross-section

4.6 Parametric Relations:

4.6.1 Friction factor:

The inlet velocity across micro-channels for fixed Reynolds numbers can be calculated by the relation:

$$Re = \frac{\rho v D_H}{\mu} \tag{5}$$

The pressure drop induced for fluid flow across the channel is expressed as

$$\Delta P = P_{inlet} - P_{outlet} \tag{6}$$

For forced laminar flow across ducts, the pressure drop can be expressed in terms of dimensionless friction factor parameter. The fanning friction factor and pumping power can be determined from the numerical values of pressure drop using the following relation:

$$f = \frac{\Delta P D_h}{2\rho v^2 L} \tag{7}$$

$$P_{power} = \Delta P \dot{V} \tag{8}$$

Shah and London [26] proposed the analytical formulation of friction factor for fully developed flow inside rectangular ducts in terms of Poiseuille number.

$$P_o = fRe \tag{9}$$

Where Poiseuille number in terms of aspect ratio is given as

$$P_o = 24(1 - 1.3553\alpha + 1.9467\alpha^2 - 1.7012\alpha^3 + 0.9564\alpha^4 - 0.2537\alpha^5) \tag{10}$$

And the aspect ratio is given as

$$\alpha = \frac{h}{w} \tag{11}$$

In case of developing flows inside rectangular channels the Poiseuille number proposed by Shah & London[26] is given as

$$P_{o\,lam}(x^+) = \left(\frac{3.44}{\sqrt{x^+}} + \frac{(fRe)_{fd} + \frac{K(\infty)}{4x^+} - \frac{3.44}{\sqrt{x^+}}}{1 + \frac{C'}{x^{+2}}}\right) \tag{12}$$

Where the values of K(∞) and C' may be obtained from ref. [26], while the dimensionless co-ordinate x^+ is given as

$$x^+ = \frac{x}{D_H Re} \tag{13}$$

The Darcy friction factor relation for rectangular channels proposed by Blevins[49] is given as

$$f = \frac{64}{Re[\frac{2}{3} + \frac{11h}{24w}\left(2 - \frac{h}{w}\right)]} \tag{14}$$

The above mentioned darcy friction factor relation to fanning friction factor is given as

$$f_d = 4f_f \tag{15}$$

The rectangular channel friction factor relation proposed by Bejan[50]

$$f = \frac{24(H_{ch}^2 + W_{ch}^2)}{Re(H_{ch} + W_{ch})^2} \tag{16}$$

The validation of numerical friction factor was performed against all of the above mentioned friction factor relations.

4.6.2 Nusselt Number

The generalized Nusselt number relation is given as

$$Nu_{avg.} = \frac{h_{avg.}D_H}{k} \tag{17}$$

The Nusselt number relation for fully developed flow across rectangular channels proposed by Shah and London[26] is given as

$$Nu = 7.541(1 - 2.610\alpha + 4.970\alpha^2 - 5.119\alpha^3 + 2.702\alpha^4 - 0.548\alpha^5 \tag{18}$$

Where α is the aspect ratio of the channel given by Eq. 11 of the previous section and the dimensionless axial length is expressed as

$$x^+ = \frac{x}{D_H RePr} \tag{19}$$

The heat transfer coefficient (h) can be represented in the total heat form as

$$h = \frac{Q}{A_{ht}\Delta T} \tag{20}$$

Where ΔT the temperature difference between base and operating fluid. The heat flux for this condition is given as

$$Q = \dot{m}C_p(T_o - T_i) \tag{21}$$

The energy balance characterizing flow through channel, with assumptions discussed in previous section, can be expressed as

$$C_p(T_o - T_i) = hA_{ht}\left(\frac{(T_o - T_i)}{\ln\left(\frac{(T_w - T_i)}{(T_w - T_o)}\right)}\right) \tag{22}$$

From the above mentioned data, As discussed in ref. [51] the Nusselt number can be formulated as

$$Nu = \left(\frac{D_H}{k}\right)\ln\left(\frac{(T_s - T_i)}{(T_s - T_o)}\right)\left(\frac{\dot{m}C_p}{A_{ht}}\right) \tag{23}$$

4.6.3 Nano-fluids

Nano-fluids are usually characterized through different numerical and experimentally determined models. However, for the present study we have utilized the thermal conductivity and viscosity of correlations formed through regression of experimental data. The R^2 values of these models were found to be 98%. The density of nano-fluids can be determined in the form of a physical mixture of fluid and particles, which can be expressed as

$$\rho_{nf} = (1 - \varphi)\rho_{bf} + \varphi\rho_p \tag{24}$$

Where the subscripts "p" and "bf" are for particle and base fluid respectively. The specific heat capacity of nano-fluid is expressed in the form of a thermal equilibrium equation between base fluid and nanoparticles.

$$\left(\rho C_p\right)_{nf} = (1 - \varphi)\left(\rho C_p\right)_{bf} + \varphi\left(\rho C_p\right)_p \tag{25}$$

The generalized relations for viscosity are given in terms of

$$\mu_{nf} = (\mu_f)\,(1 + a\varphi + b\varphi^2) \tag{26}$$

However, for accurate prediction of results, we are interested in the experimentally formulated relations of nano-fluids. Therefore, for aluminum-oxide particles and base fluid combination, the above mentioned equation was expressed giving following expressions[45].

$$k(\varphi, T) = k_f(T)(1 + 4.5503\varphi) \tag{27}$$

$$\mu_{al}(\varphi, T) = \mu_f(T)\; exp[4.91\varphi/(0.2092 - \varphi)] \tag{28}$$

For the KKL model the equations can be expressed as a combination of static and Brownian motion of particles, Therefore the thermal conductivity and viscosity of nano-fluids for this model is given as

$$k_{eff}{}_{nf} = k_{static} + k_{Brownian} \tag{29}$$

$$\mu_{eff_{nf}} = \mu_{static} + \mu_{Brownian} \quad (30)$$

The static part of thermal conductivity equation can be expressed in the form of Hamilton-Crosser model.[52]

$$(k)_{nf} = \left[\frac{(k_p + 2k_f) - 2\varphi(k_f - k_p)}{(k_p + 2k_f) + \varphi(k_f - k_p)}\right] \times k_f \quad (31)$$

Where k_f and k_p are the thermal conductivities of base fluid and nanoparticles respectively.

$$k_{brownian} = 5 \times 10^4 \alpha C_{p_{bf}} \rho_{bf} \sqrt{\frac{K_b}{d_{np}\rho_{np}}}\, g(T, \alpha, d_{np}) \quad (32)$$

Where K_b is the Boltzmann constant, while the α and ρ_{np} are the volume fraction and nano-particle density respectively. The function $g(T, \alpha, d_{np})$ provided by the KKL model[53] can be expressed as

$$\begin{aligned} g = {} & \left(a + b\ln(d_{np}) + c\ln(\alpha) + d\ln(\alpha)\ln(d_{np}) + e\ln(d_{np})^2\right)\ln(T) \\ & + \left(m + h\ln(d_{np}) + i\ln(\alpha) + j\ln(\alpha)\ln(d_{np}) + k\ln(d_{np})^2\right) \end{aligned} \quad (33)$$

The values of co-efficient were obtained from ref. [53]. The effective nano-particle thermal conductivity can be obtained from the following relations.

$$R_b + \frac{d_p}{k_p} = \frac{d_p}{k_{np,eff}} \quad (34)$$

The static and dynamic parts of viscosity can be calculated as [54]

$$\mu_{static} = \frac{\mu_{bf}}{(1 - \alpha^{2.5})} \quad (35)$$

$$\mu_{brownian} = 5 \times 10^4 \alpha \rho_{bf} \sqrt{\frac{K_b T}{d_{np}\rho_{np}}}\, g(T, \alpha, d_{np}) \quad (36)$$

4.6.4 Evaluation Parameters

The efficiency of micro-channels can be expressed as a ratio of Nusselt number obtained for novel design over the Nusselt number for conventional straight channel and the same approach can be used for pressure drop efficiency as discussed in [55]

$$e_{Nu} = \frac{Nu_{Hybrid}}{Nu_{Straight}} \quad (37)$$

$$e_f = \frac{\Delta P_{Hybrid}}{\Delta P_{Straight}} \tag{38}$$

Harikrishnan [56] used the following thermal performance parameter for overall evaluation of design.

$$TPF = \frac{Nu/Nu_o}{(f/f_o)^{1/3}} \tag{39}$$

However, since the design of interacting channel gives lowering of localized outlet temperatures, therefore for fair comparison between the two designs can be established for cooling effect delivered at the base therefore the new parameter for TPF comparison between different design is given as

$$TPF(cooling) = \frac{\Delta T_{Hybrid}/\Delta T_{Straight}}{(f/f_o)^{1/3}} \tag{40}$$

CHAPTER 5: RESULTS AND DISCUSSION

5.1 Grid Independence:

The Meshing module available in ANSYS was used to generate a non-uniform structured mesh with hexahedral elements. The mesh across the inlet/outlet cross sections was refined with bias factors to achieve better accuracy of results across the boundary regions as shown in **Fig. 6**. Grid independence studies were performed for different mesh sizes in order to achieve stabilization of results. The mesh was varied from coarse to fine with increasing number of elements until a stable solution with an acceptable numerical error was achieved. Thus a condition was reached where large changes in mesh density led to negligible changes in numerical calculations results. The Reynolds number of 500 was taken as reference parameter for grid independence as a mean value over the Reynolds number range (100-1000). The mesh was improved from coarse to very fine with the increase in number of elements. The analytical result of friction factor was plotted against the number of elements as shown in **Fig. 7**. The results were found to be in good agreement with analytical solutions and a maximum error of 10% in the pressure drop, arising at very high Reynolds number in case curved channels, which can be explained to be a consequence of introduction of curve across the length of micro-channel. The results have been plotted against number of elements shown in **Fig. 7** and the details are discussed in **Table 6**.

Table 6: Grid Independence

S. No.	Number of Elements	Friction Factor		Error (%)
		Present Study	Shah & London [26]	
1	22500 (very coarse)	0.03528	0.0412	14.30
2	45000 (Coarse)	0.037195	0.0412	9.64
3	87500 (Coarse)	0.038182	0.0412	7.25
4	168000 (Fine)	0.040658	0.0412	1.23
5	320000 (Fine)	0.041424	0.0412	0.62
6	600000 (Fine)	0.042564	0.0412	3.39
7	1080000 (very Fine)	0.042706	0.0412	3.73
8	2160000 (very Fine)	0.042758	0.0412	3.86
9	4320000 (very Fine)	0.042792	0.0412	3.94

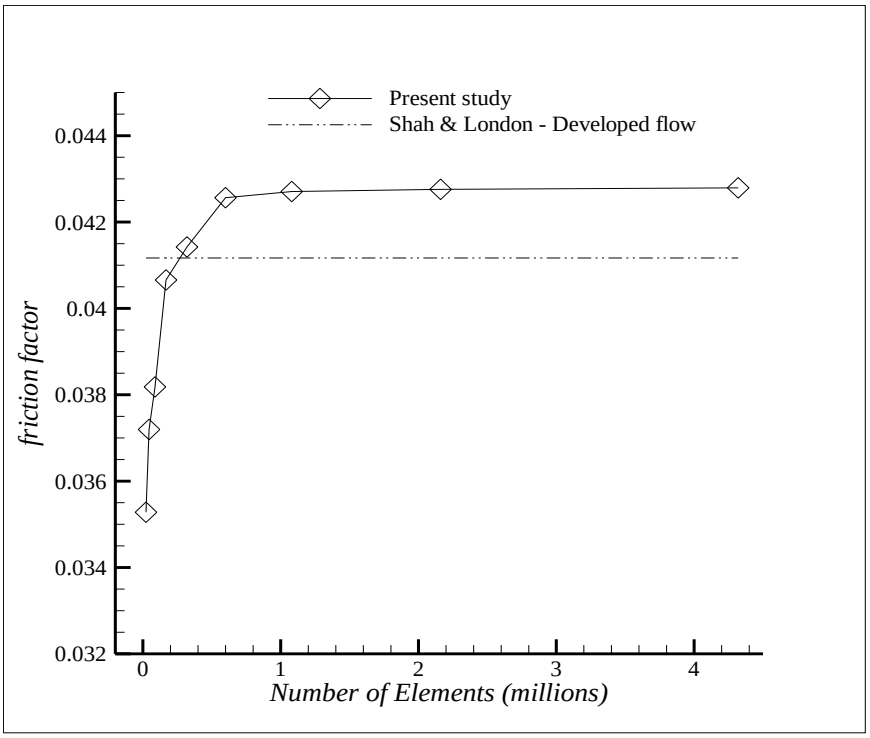

Fig. 7: Bended Channel Grid Independence

5.2 Validation:

The validation of numerical results was performed through comparison with established analytical relations available in literature. The validated data was further confirmed through the estimation of entrance length, Nusselt number and dimensionless pressure drop to determine the accuracy of results. The shah and London[26] relation for Nusselt number was used to validate the Nusselt number as shown in **Fig. 8**.

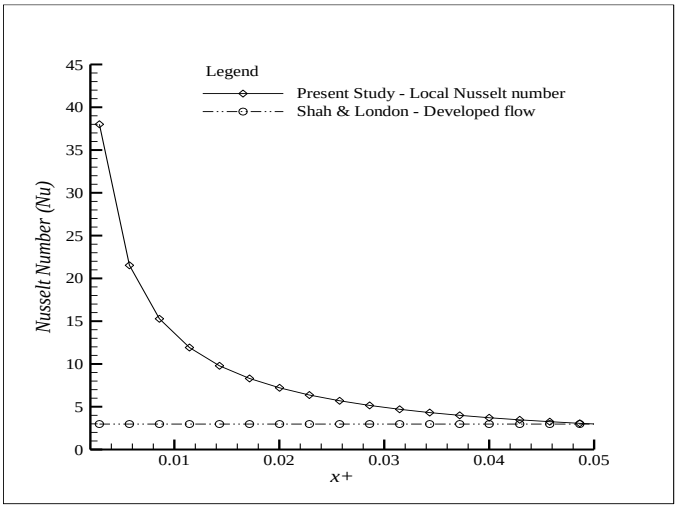

Fig. 8: Nusselt number validation

It can be seen that the localized value of Nusselt number is very high at the initial portion along the length of the channel as the hydrodynamic profile of fluid flow is not fully developed, however the flow becomes fully developed as it reached the end of the channel and the Nusselt number value stabilizes to a value close to the solution provided by Shah and London [26]. The analytical relations for Nusselt number and friction factor given by Shah and London for both developed and developing flow have been given in the previous section. However, since the flow is with a combination of hydrodynamically developing and developed flow, therefore the results were also compared against the developing relation of Shah and London. Reliable analytical relations for friction factor were also developed by Blevins (1984) and Bejan (2013) and they have also been used to validate our results.

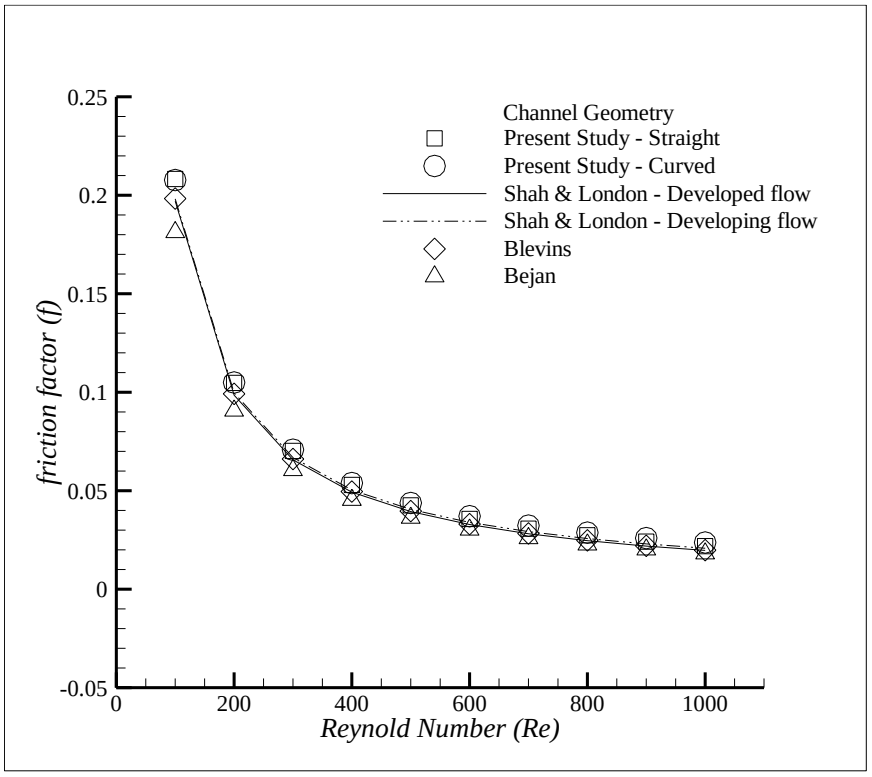

Fig. 9: Validation at aspect ratio 0.167

The numerical solution of friction factor shows good agreement with Shah and London[26] as well as Blevins[49] relations for fully developed flow at low aspect ratio as shown in **Fig. 9**. An error of less than 6 percent was observed for the numerical results which can be explained in terms of the pressure loss associated with the initial flow development region. However it has been shown that the Bejan[50] correlation underpredicts the friction factor against low values of Reynold numbers, however beyond 200 Reynold numbers it shows good agreement with

numerical results. The results were also validated for aspect ratio of 1 as shown in **Fig. 10** it can be seen that fully developed equations hold good for low Reynolds numbers, however for flows at Re =1000, it was shown that the error with fully developed equations becomes higher while the error with developing equation becomes less thus proving that developing flow regime dominates a major portion of flow at higher Reynolds numbers. The friction factor values for curved channel geometry, as shown in **Fig. 10** also show better agreement with developing flow relations throughout all values of Reynolds numbers showing that for curved channels, developing flow dominates the major portion of channel flow.

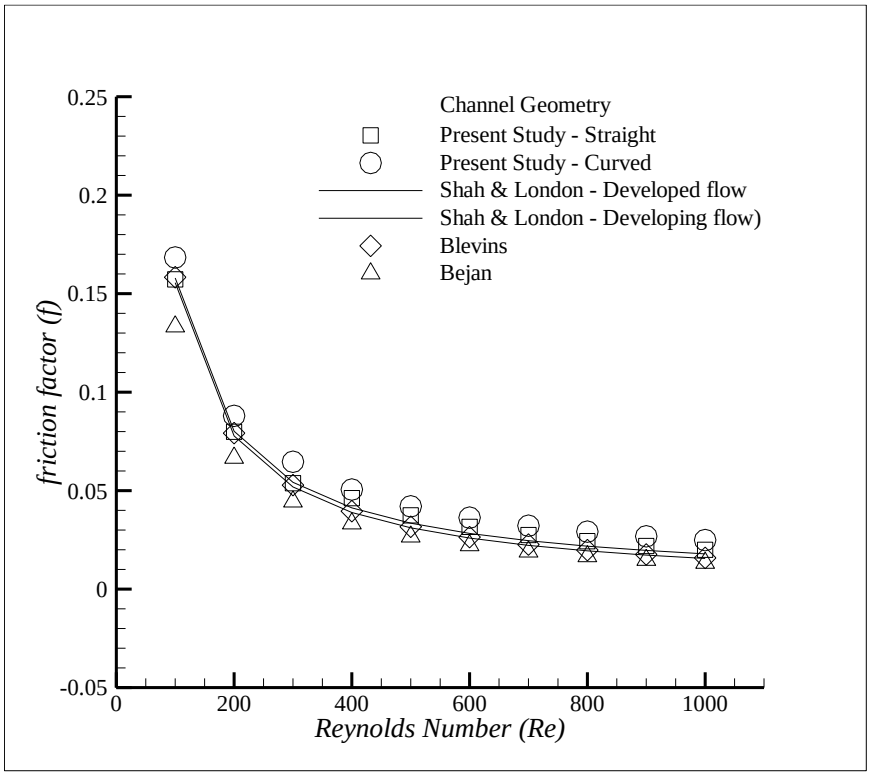

Fig. 10: Validation at aspect ratio 1

5.3 Aspect Ratio:

Straight channels of varying aspect ratios were modeled using the temperature dependent thermo-physical properties of de-ionized water. Initially the optimum aspect ratio of straight micro-channels was studied. The parameters of width and height were varied against a fixed channel length of 18mm. This length was determined according to the side length of a square lab on chip application for which the solution is being proposed. The optimized design points for each geometry were finalized using the friction factor and Nusselt number parameters. This

optimization was based on design point method where the friction factor and Nusselt number were plotted against increasing Reynolds number and the point of intersection between these two curves was adopted as the most efficient design point according to that specific geometry. The optimization was based on design point criteria, where performance of optimum points for each geometry were compared. The selection criteria was based upon the convergence of solution values to a state where a difference in absolute value of less than 1×10^{-1} was achieved for both the Nusselt number and friction factor. Therefore, the stabilization of pressure drop and Nusselt number at value of 1×10^{-1} was achieved. The width of the channels was fixed and multiple aspect ratios were investigated against each geometry to find the most efficient design with the highest convective heat transfer characteristics. These steps were repeated for three separate boundary Temperature conditions. The results obtained from different aspect ratios are given in **Fig. 11** and **Fig. 12**.

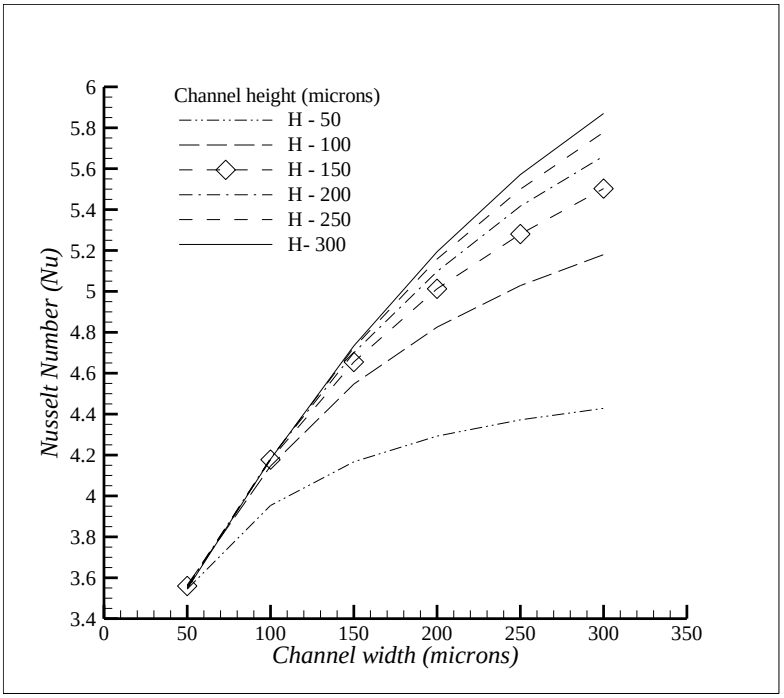

Fig. 11: Nusselt Number for different aspect ratios

Channels of varying aspect ratios were studied by varying the width and height of micro-channel geometry between a range of 50 microns to 350 microns and the best performing channel in terms of Nusselt number was finalized to further enhance its performance through fluid mixing. From the above mentioned design selection criteria and the resulting numerical values, a channel of aspect ratio 1 and a base width of 300 microns provides us with the best

performance. However going beyond this width is not feasible as the increase in width provides negligible change in Nusselt number. Further, it has been shown through research that for cooling of surface it is preferable to have a higher number of channels therefore going beyond this limit might negatively affect the multichannel performance. Also the channel would change scale from being micro-scale to mini-scale and thus not providing the required intimate contact of fluid with surface. Therefore, in light of the above mentioned data, the channel design was varied through the introduction of curve and base corrugation to enhance its overall performance.

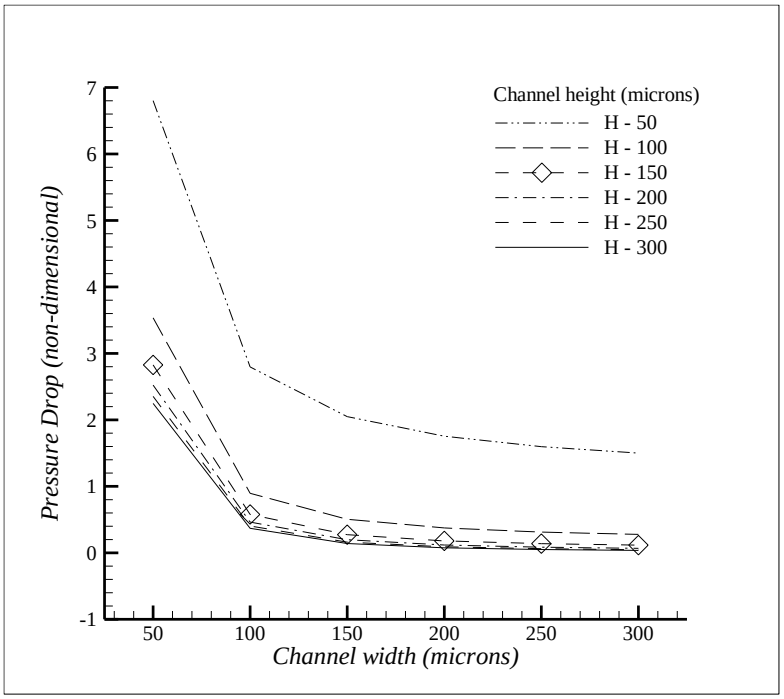

Fig. 12: Dimensionless Pressure drop for different aspect ratios

5.4 Bended-Corrugated Channels:

After finalization of optimum aspect ratio of straight channels. Bends of varying angles were studied for a range of 0° to 90°. For such cases, the curvature induces a centrifugal effect on fluid flow thus producing imbalance in velocity gradient. This instability, known as Dean instability, leads to fluid recirculation across the curve. A total of six test cases were initiated with periodic increments of 15° to obtain Nusselt number and friction factor against each bend. The details of these micro-channels have been provided in **Table 7**.

Table 7: Bended angle geometries

S. No.	Width (microns)	Height (microns)	Bend Angle (degrees)
1	300	300	15
2	300	300	30
3	300	300	45
4	300	300	60
5	300	300	75
6	300	300	90

The multi objective response optimization of bended channel was carried out using angle "θ" as a continuous variable with the pressure drop and Nusselt number as the response variables. The optimized angle with a composite desirability of 0.83 was finalized as the optimum bend angle. The resulting surface plot of optimization and response variable is shown in **Fig. 13**. The angle obtained from optimization was validated by plotting the friction factor and Nusselt umber against increasing Reynold number and the point of intersection between these two curves was adopted as the most efficient design point according to that specific geometry.

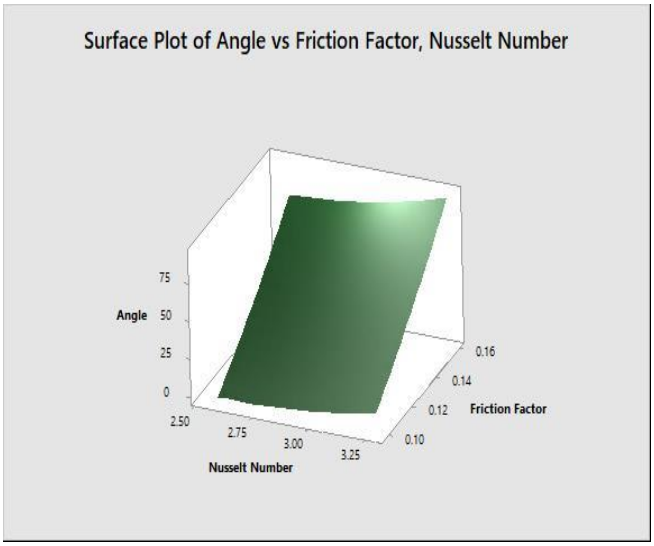

Fig. 13: Response Surface plot

The optimized bend angle was further improved with the removal of sharp corners from the bended geometry. The bend was replaced by an equivalent curve which provided equivalent Nusselt Number and friction factor values. The data shown in **Fig. 14** and **Fig. 16** present the dimensionless outlet temperature and pressure drop respectively, where a negligible difference in both values were observed for bended and curved channels.

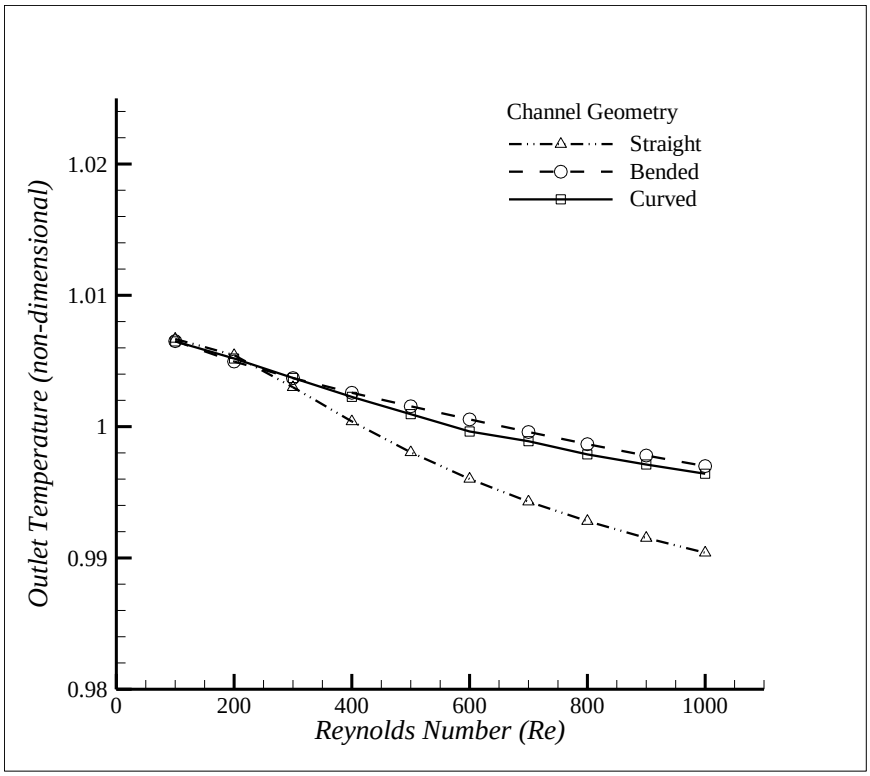

Fig. 14: Dimensionless outlet temperatures

The resulting data from bended channel was used to obtain a regression model for Nusselt number and pressure drop in terms of continuous variable "θ". The accuracy of these regression models is beyond 99%. Therefore the characteristic equations for bended channels at optimized Reynolds number values with de-ionized water having temperature dependent properties can be expressed as

$$Nu = 5.6180 + 0.02060\boldsymbol{\theta} - 0.000155\boldsymbol{\theta}^2 \quad (35)$$

$$PD = 193134 + 1347\boldsymbol{\theta} - 0.\ 5\boldsymbol{\theta}^2 \quad (36)$$

These equations are also applicable for curved channel models where the dimensionless outlet temperature and pressure drop is approximately same as shown in **Fig. 14** and **Fig. 16** respectively. The flow phenomenon for straight as well as bended channel for Reynolds number 500 and 1000 is shown in **Fig. 15**.

Re = 500

Re = 1000

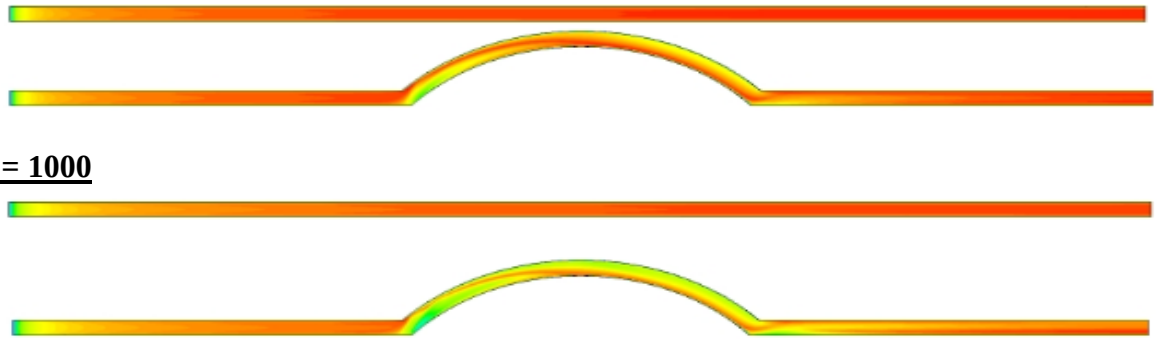

Fig. 15: Flow phenomenon

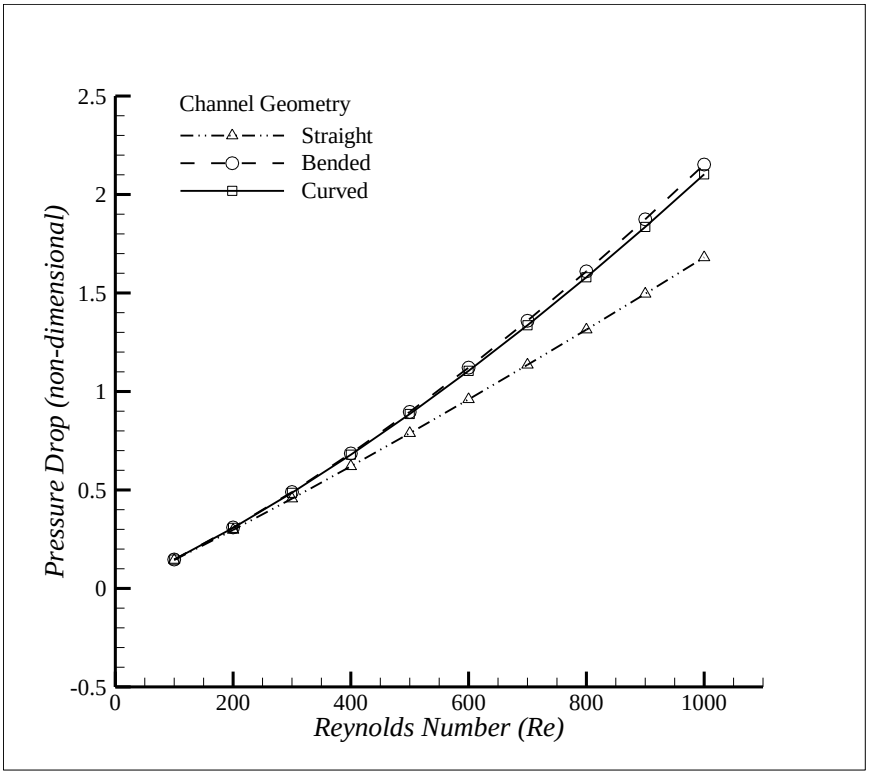

Fig. 16: Dimensionless pressure drop

The flow phenomenon across curved channel leads to generation of dean vortices at different Reynolds numbers of 500 and 1000, which can be seen in **Fig. 15**. The same dean cortices were also generated across bended channel geometries and the noticeable increase in convective heat transfer and pressure drop at Reynolds number beyond 300 is linked to this phenomenon. The dean vortices across the curve at Reynolds number of 1000 as shown in **Fig.**

17 are characterized by a corresponding Dean number. The dean number is given as $De = Re\sqrt{\frac{D_H}{2R}}$. In our case of optimized bend the dean number comes out to be De = 203.9.

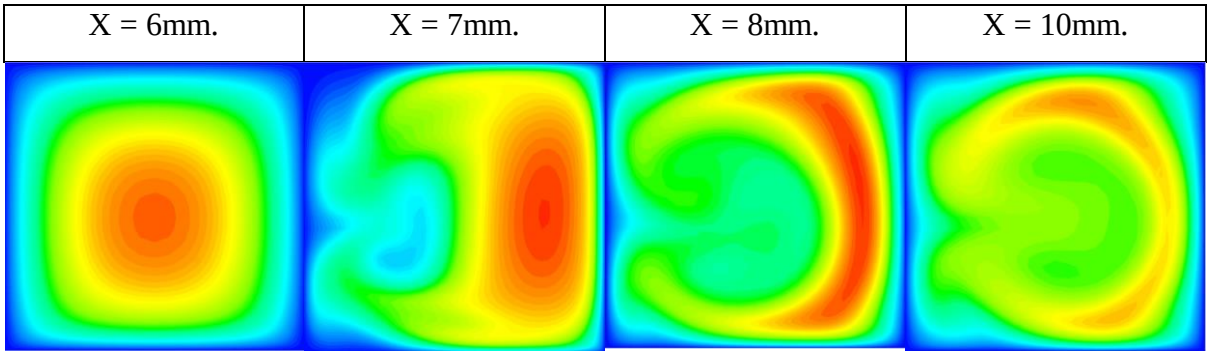

Fig. 17: Dean Vortices across the curve

The bended and curved channel show fluid mixing due to generation of dean vortices. However, it is desirable to have continued flow disruption in the fluid at the bottom of the channel to enhance heat transfer rates. Therefore, a corrugation pattern was adopted for heat transfer enhancement at the base of the channel. The proposed corrugation is based on a periodic diverging-converging pattern as shown in **Fig. 18**. The width, length and depth of corrugation pattern was studied in the form of three separate design parameters. The design parameters were identified as width ratio and aspect ratio. The parameters can be defined as: $Width\ ratio = \frac{W_{min.}}{W_{max.}}$ and $Aspect\ ratio = \frac{H}{W_{Avg.}}$, where A is defined as $A = W_{avg.} = \frac{W_{max}+W_{min}}{2}$.

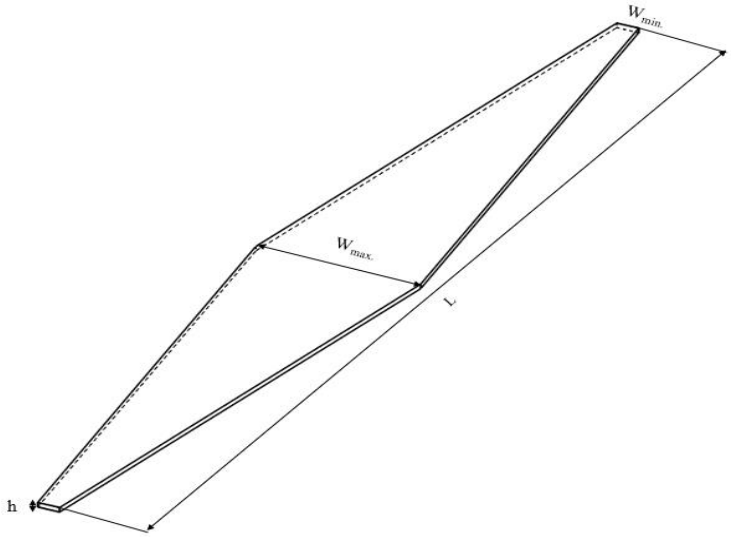

Fig. 18: Diverging-Converging corrugation model

The study of channel cross section in case of curved channels as compared to curved corrugated channel shows the enhanced heat transfer performance of channel with corrugated base. This can be attributed to the flow disruption effect that occurs at the base of the channel due to the diverging-converging pattern of flow near the heated wall resulting in higher values of conjugate heat transfer. The temperature contours of channel cross section are shown in the **Fig. 19**.

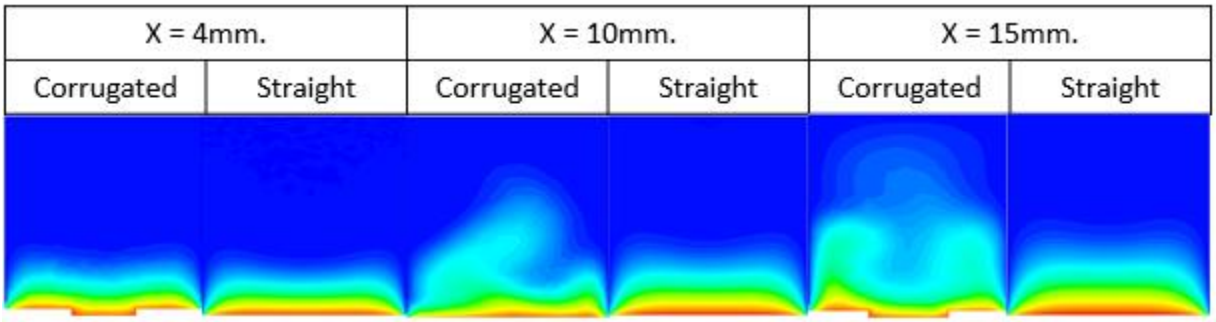

Fig. 19: Channel Cross section comparison of flat and corrugated base

The comparison shown in **Fig. 20** shows that a decreasing width ratio shows improved Nusselt number and friction factor. The decreasing width ratio shows the difference in maximum and minimum width values of this model. Therefore the difference between maximum and minimum width dimensions should be maximum to achieve the best results as shown in the figure below

Fig. 20: Width ratio comparison at base of channel

The friction factor and Nusselt number values for the same width ratios can be seen in **Fig. 21**. Where a lower value of width ratio corresponding to bigger difference between maximum and minimum width sizes has been shown to provide improved heat transfer rates across the channel.

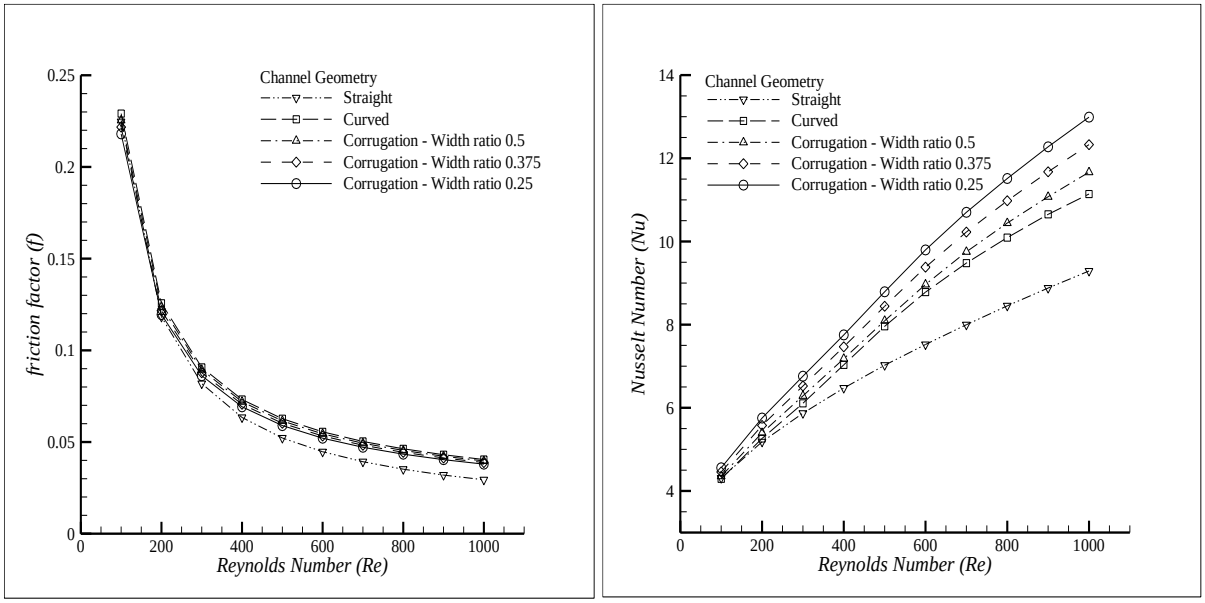

Fig. 21: Variation of Nusselt number and friction factor with width ratio

The increase in depth of the channel shows improved heat transfer rates and less pressure drop as compared to same corrugation pattern with smaller height. This is shown in the **Fig. 22**, given below

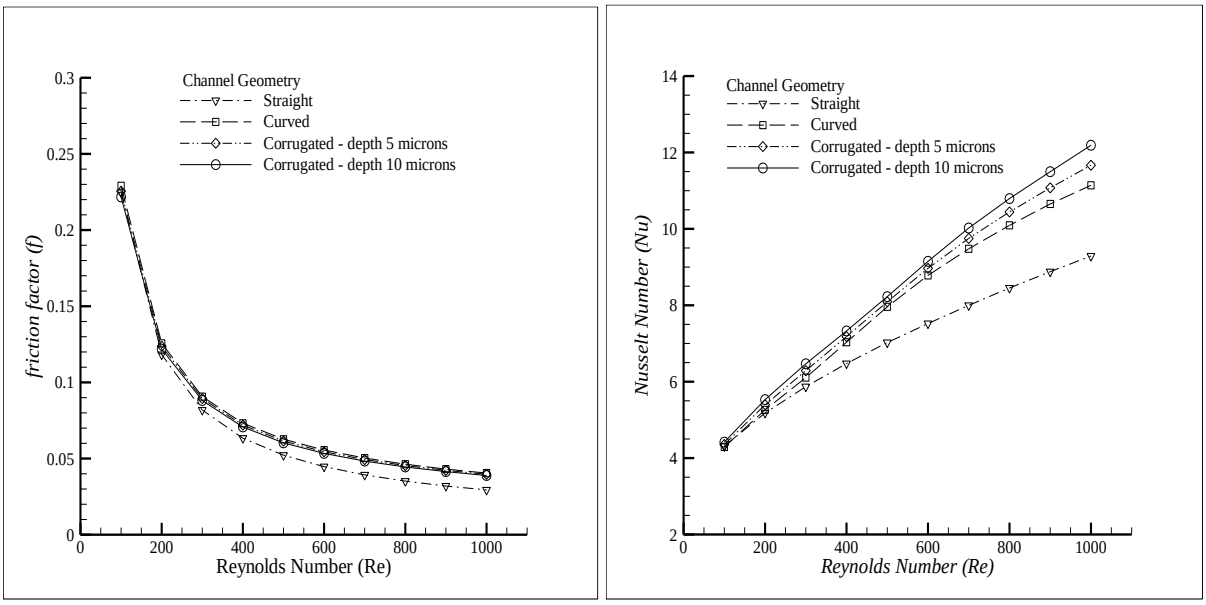

Fig. 22: Variation of Nusselt number and friction factor with aspect ratio

Therefore the corrugation height of 10 microns was chosen as the reference height f base corrugation. The comparison of different width ratios was expressed in terms of Nusselt number nad friction factor efficiency of the channel. The efficiency is shown in **Fig. 23**. Where we can observe the superior performance of channels with lower width ratios.

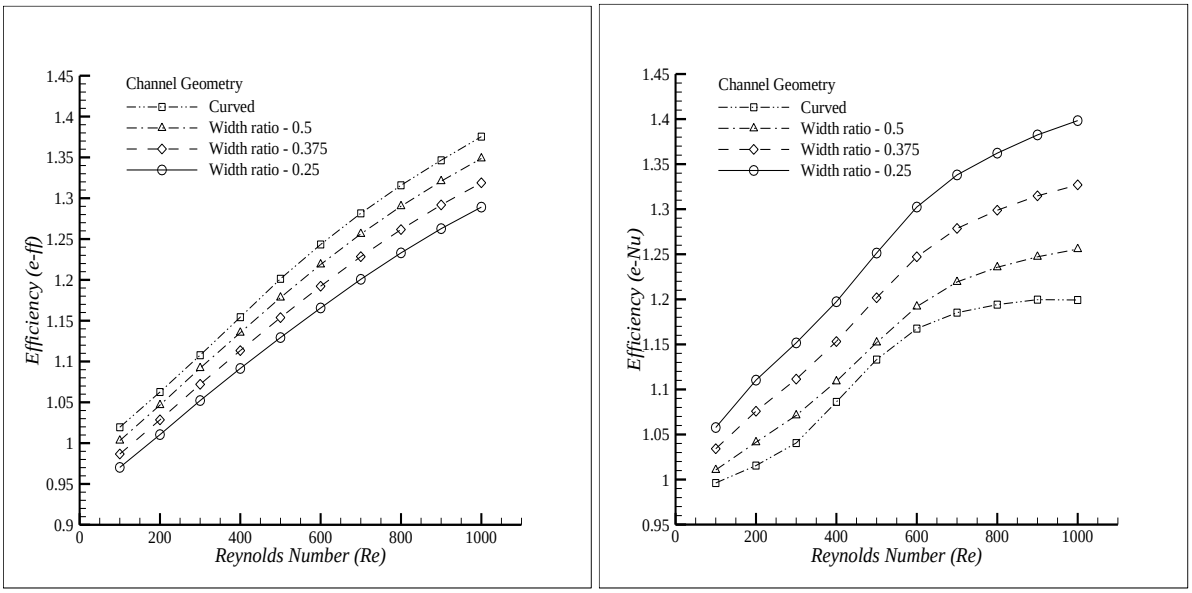

Fig. 23: Nusselt number and friction factor efficiency

The overall thermal performance factor given in Fig. 20 shows the efficiency of curved corrugated channels over curved and conventional straight channel geometries.

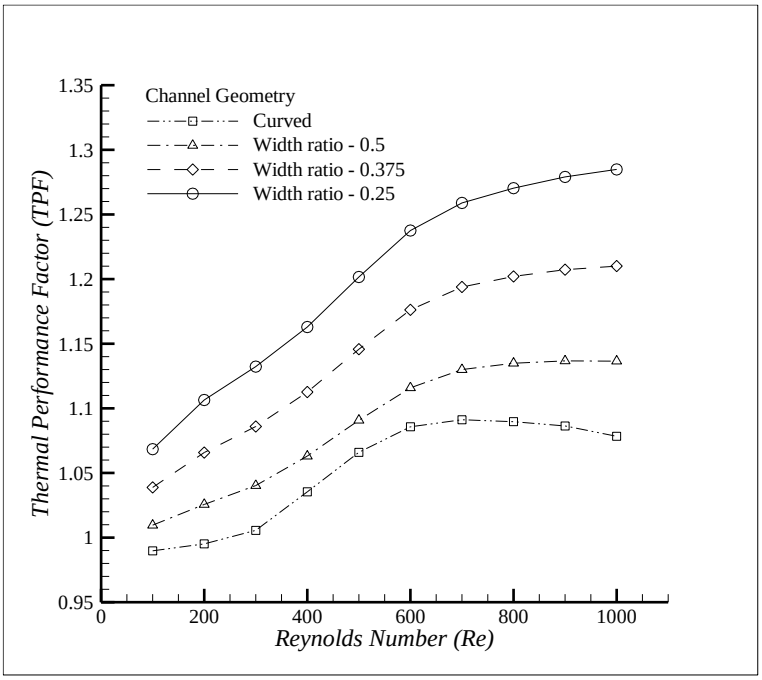

Fig. 24: Overall thermal performance factor for corrugated curved channel

The addition of nano-particles to the de-ionized water was studied for the curved-corrugated channel and dual interacting channel geometries. The performance of most commonly used aluminum oxide nano-particles was compared against two separate models proposed by Rea et al. and KKL models. The reference parametric relations for nano-fluids have been discussed in chapter 4. Using the mentioned equations we formulated the thermo-physical properties of the new nano-fluids. The resulting effect of increase in Nusselt number and friction factor is given in **Fig. 25**. This shows the improved heat transfer properties of nano-fluids. However, we observe that the Rea model under predicts the results in comparison to KKL model for the same particle concentration, therfoe we conclude that the rea model is geometry dependent and cannot be used as a generalized relation in comparison to KKL models.

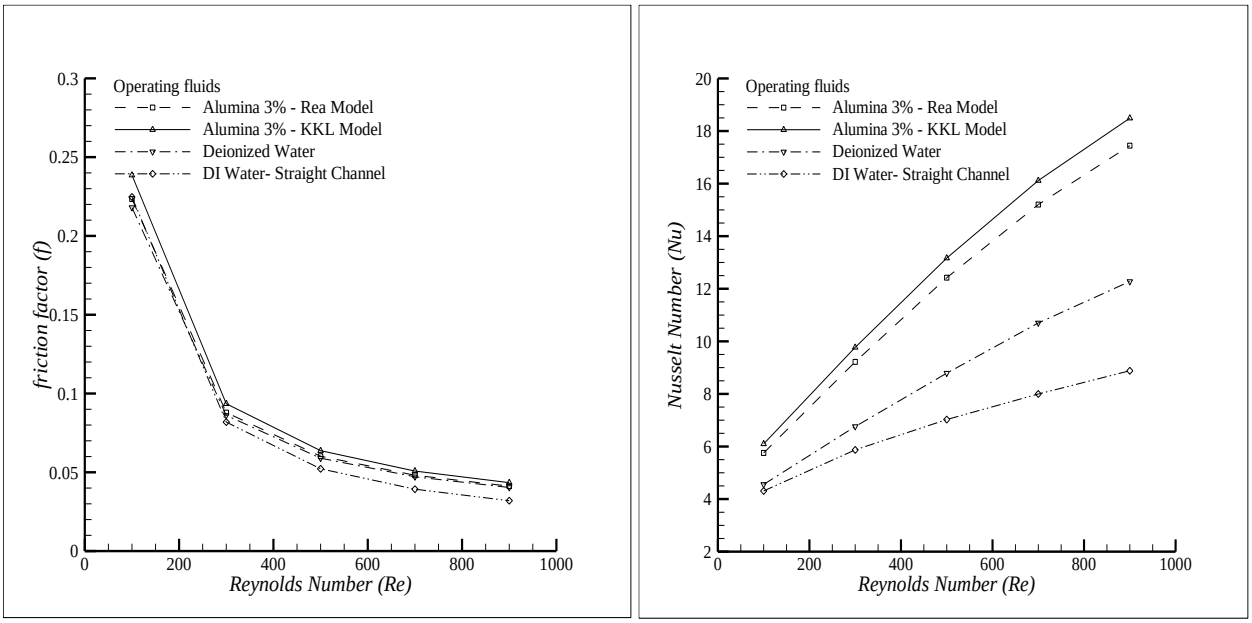

Fig. 25: Nusselt number comparison for KKL and Rea Model

5.5 Interacting-Corrugated Channels:

A connecting bridge of varying width was introduced between two parallel channels to induce flow mixing and increase convective heat transfer. The orientation of connecting bridge was varied from optimum angle of 35° to 90° in order to determine the effect of changing bridge angle upon fluid mixing and performance parameters. Both straight channels and curved channels with corrugation were used as reference geometries. The flow phenomenon was varied from parallel flow type to counter flow type for extensive study. The simulation matrix is given in the **Table 8**.

Table 8: Simulation Matrix for interacting channels

S. No.	Width (microns)	Height (microns)	Angle (degrees)	Geometry	Flow
1	300	300	90°	Straight Channel	Parallel and Counter flow
2	300	300	35°	Straight Channel	
3	300	300	90°	Curved Channel	
4	300	300	35°	Curved Channel	

Based on the results of the simulations matrix given by **Table 8**, it was found that interacting straight channels for a 90° connecting bridge provide us with the best results. Therefore, the finalized model was further studied for variation in bridge width and flow types to determine the best results. The simulation results of parallel and counter flow phenomenon provided us with re-circulations regions and counter rotating vortices. The flow phenomenon for Serial No. 1 at Re = 1000 have been shown in **Fig. 26**.

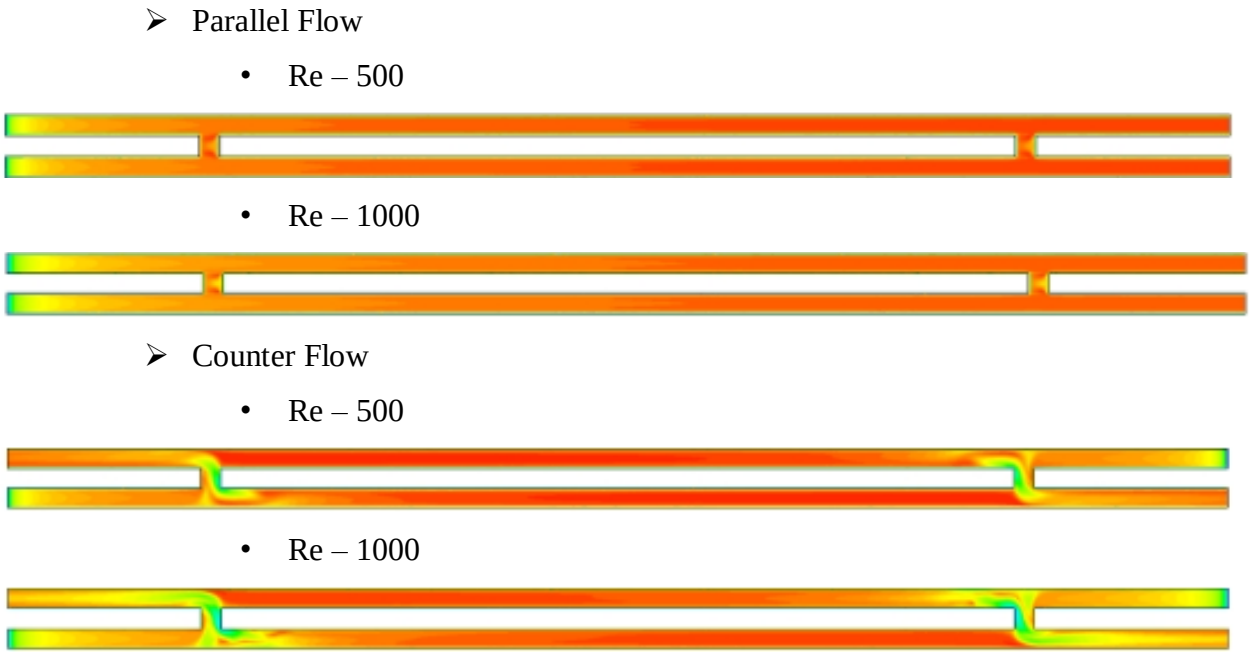

Fig. 26: Interacting Channel flow phenomenon

Therefore, the finalized best performing geometry with a connecting bridge of 90° was simulated for different bridge width as well as parallel and counter flow conditions as given by the simulation matrix given in **Table 9**.

Table 9: Simulation Matrix for straight interacting channels of varying bridge width

S. No.	Width (microns)	Height (microns)	Angle (degrees)	Geometry	Bridge width	Flow type
1	300	300	90°	Straight Channel	W	Parallel and Counter
2					1.5 W	
3					2 W	

The geometries given in the above table were numerically studied and it was found that the outlet temperature for counter flow cases is slightly lower than the outlet temperature for parallel flow cases at very low values of Reynolds numbers. However the cooling effect at the base for counter flow phenomenon was significantly higher as compared to parallel flow cases. This decrease in outlet temperature can be explained by the fact that as the fluid moves close to the outlet of one channel, the incoming cool fluid of the parallel channel mixes increasing the local Nusselt number while also decreasing the outlet temperature. Therefore, a fair comparison between two models of varying flow direction can only be made by using the overall cooling effect of channels. The flow phenomenon along with bridge phenomenon for parallel and counter flow cases can be seen in the **Fig. 27** and **Fig. 28** respectively.

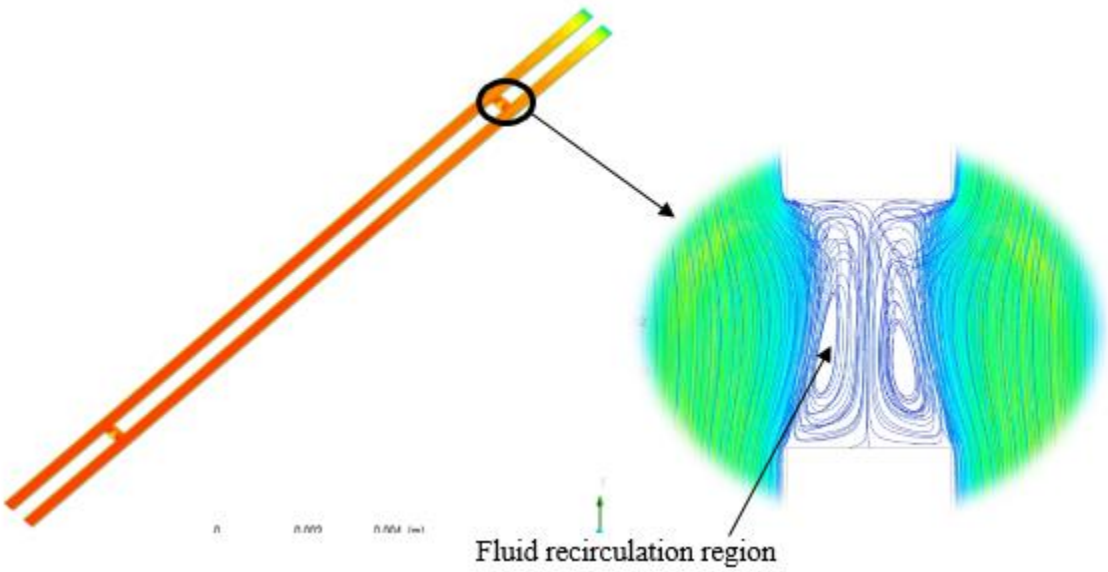

Fig. 27: Parallel flow phenomenon at bridge

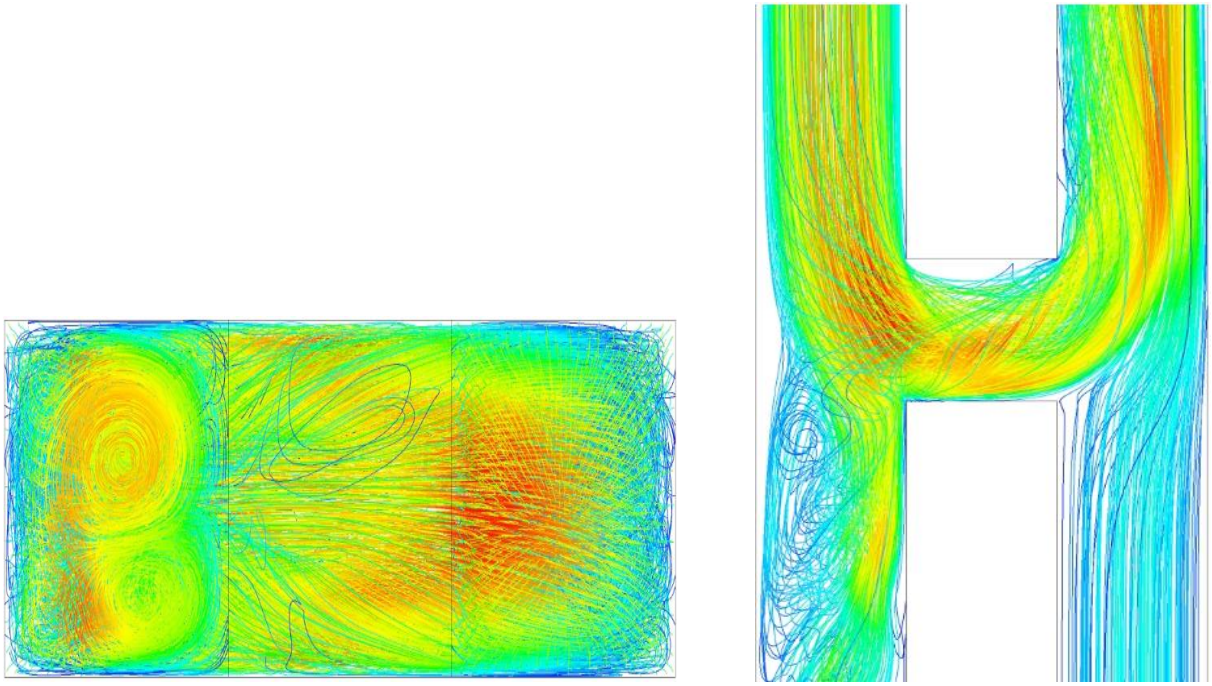

Fig. 28: Counter flow phenomenon at the Bridge

The flow phenomenon at mid-section of the flow is shown in **Fig. 29**. Where we can observe the flow recirculation zones at the bridge for parallel flow cases and flow crossing over to the neighboring channel can be seen in counter flow case.

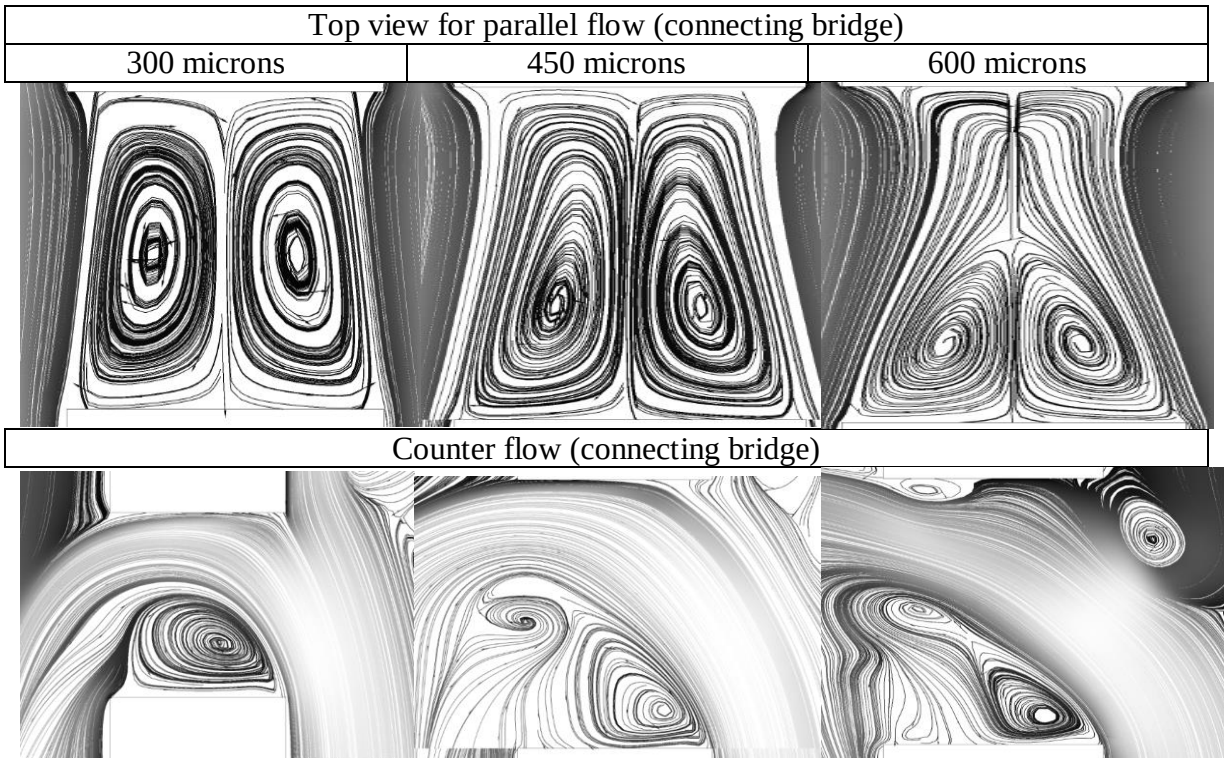

Fig. 29: Flow phenomenon at bridge (mid-section view)

The flow outlet is shown in the **Fig. 30**, where a regular flow profile can be seen at the outlet of parallel channel flow configurations of different bridge widths, however for the counter flow channel case counter rotating vortices occur at the channels outlet showing that the incidence of flow into a neighboring channel leads to counter rotating vortex phenomenon, thus explaining the higher heat transfer rates obtained for the counter flow cases.

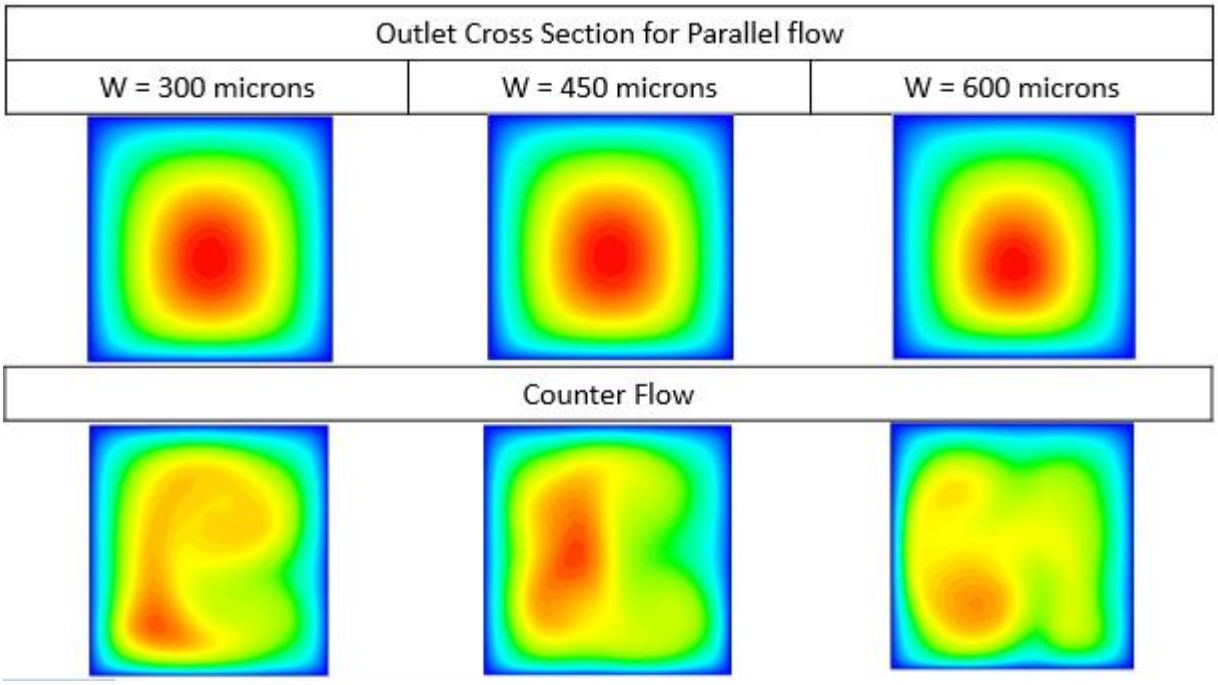

Fig. 30: Outlet cross section of interacting channels

The resulting cooling efficiency of channels as shown in **Fig. 31**.

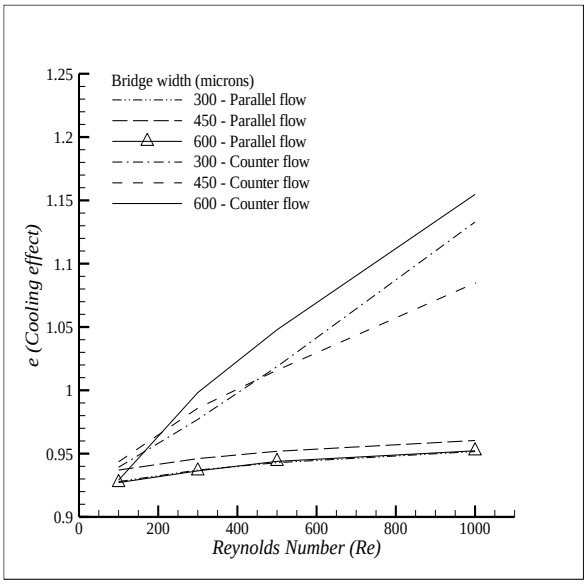

Fig. 31: Cooling efficiency for Interacting Channels

The bridge flow phenomenon can be studied for all flow conditions as given in **Table 9**. The efficiency can be expressed as the cooling effect of the geometry and the efficiency of pressure drop as discussed in the previous section. Therefore, the cooling efficiency can be seen in **Fig. 31** where an improved cooling effect can be seen for all three counter flow cases when compared against parallel flows. The results of friction factor efficiency shown in the **Fig. 32**, demonstrate the superior performance of interacting channel for counter flow phenomenon. The counter flow model outperforms parallel flow configuration for all values of bridge width in case of interacting channels. The higher cooling effect and lower value of friction factor can be seen through the relevant graphs.

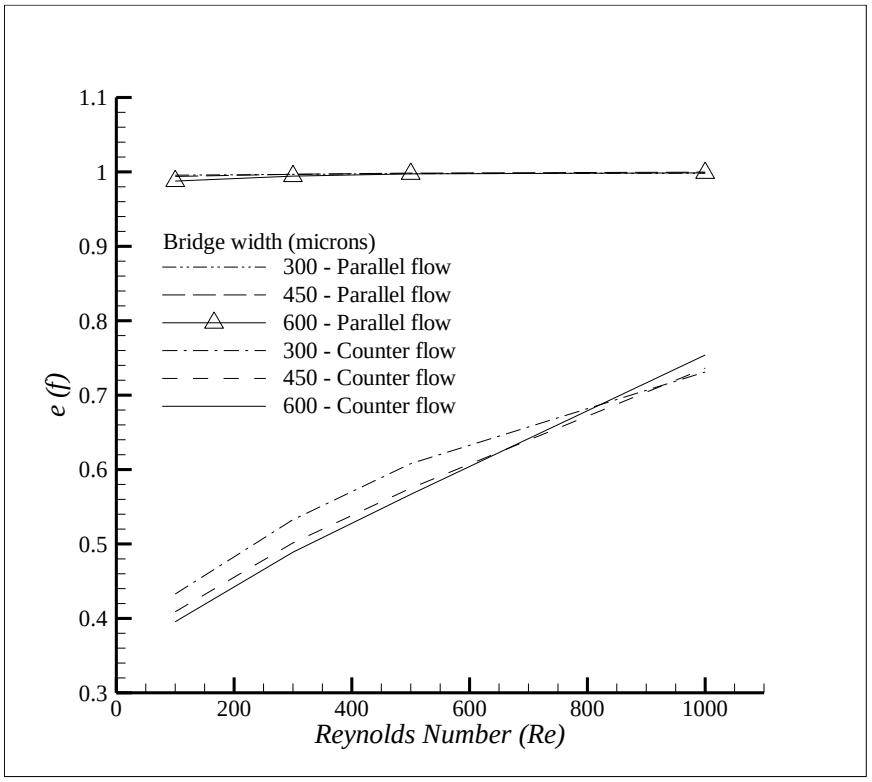

Fig. 32: Efficiency friction factor for interacting channels

There is marked reduction in pressure drop for counter flow cases when compared against parallel flows. This reduction in pressure drop is due to the crossing over of fluid and resulting flow mixing across the bridge that can be observed in counter flow scheme as compared to parallel flow cases. Consequently, the friction factor efficiency as shown by **Fig. 32**, sees a marked reduction in comparison to other flow conditions.

The TPF comparison of these interacting channels is given in **Fig. 33.**, where the parallel flow configuration provides a stable performance however the counter flow configuration provides superior performance throughout the entire range of study showing the overall comparatively superior performance of the design.

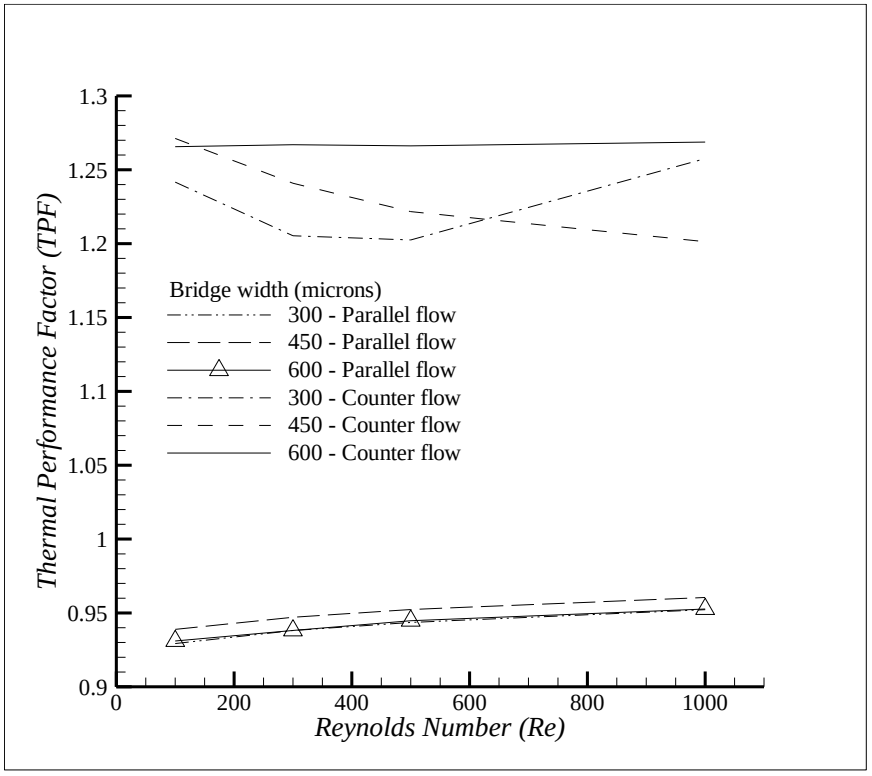

Fig. 33: TPF comparison

The graphs show major decrease in pressure drop across counter flow condition for different channels. The parallel flow cases show a consistent value of efficiency however since the desirable efficiency for friction factor is below a factor of 1. Therefore, the best geometry as shown in the **Fig. 33** for thermal performance comparison is the counter flow interacting channel model with highest bridge width.

The addition of base corrugation to these interacting channels provides a small increase in Nusselt number values against no increase in fiction factor as shown in the **Fig. 34**. Therefore, this increase in Nusselt number against no increase in friction factor is a desirable condition providing favorable heat transfer performance.

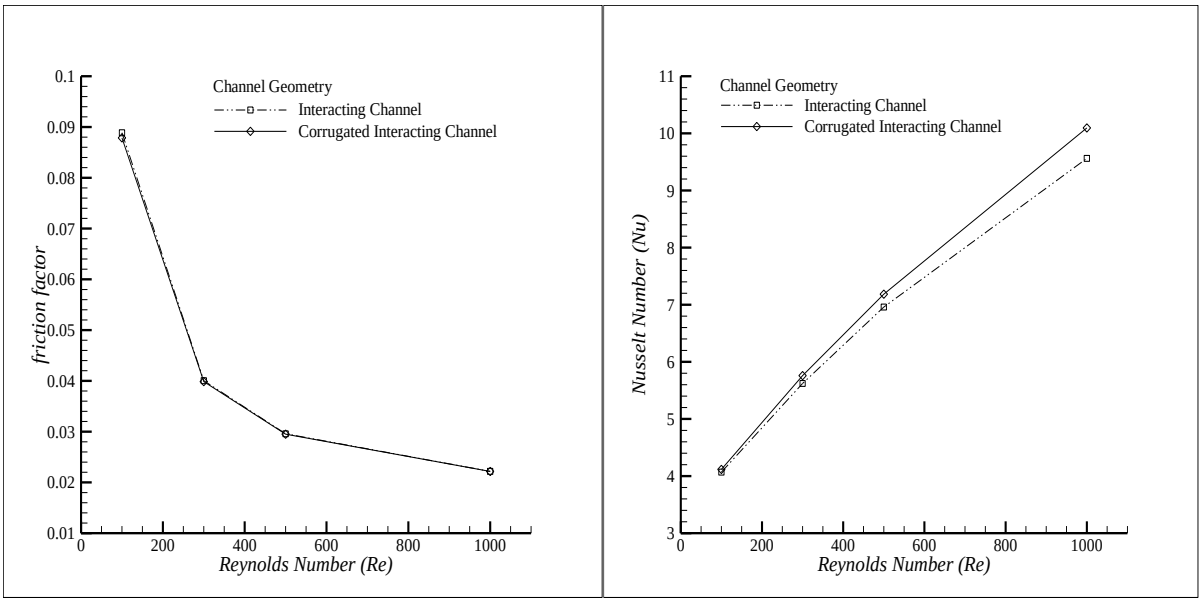

Fig. 34: Interacting Corrugated Channels

The comparative study between the Rea and KKL model given in **Fig. 35**, shows that the Rea model cannot accurately predict the performance of micro-channels since it under predicts the results by a maximum of 6%. Therefore he model can be assumed to be geometry dependent as compare d to the reliable KKL model.

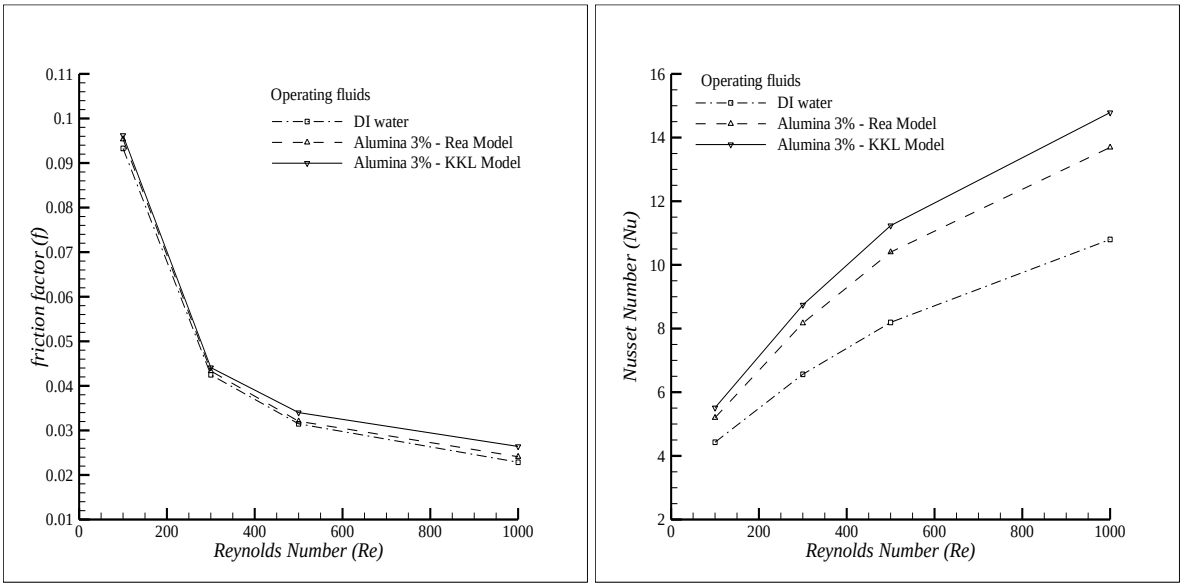

Fig. 35: Nano-fluids for Interacting corrugated channel

CHAPTER 6: CONCLUSIONS

- Introduction of bend along the length of channel generates dean vortices, thus improving the overall heat transfer rate.
- Counter rotating vortices were generating for flow across sharp corned bends of up to 90° as well as channels with connecting bridges.
- The vortex generation phenomenon also occurs in geometries other than curved channels.
- For bended and curved channels dean vortices were generated at Reynolds number beyond 300 showing that a minimum threshold velocity is needed to generate dean instability. While the same counter rotating vortices were generated for all values of Reynolds numbers in case of interacting geometry.
- The vortex generation phenomenon provides improved heat transfer rates across the length of micro-channels.
- Both models have been observed to deliver similar values of TPF, however a closer review reveals drastic differences between cases. For the curved model the increment in friction factor lags behind the increase in Nusselt number as, while for the Interacting model the Nusselt number increase lags in comparison to friction factor.
- While most of the work in this field is concentrated on flow pattern disruption or flow mixing in separate studies. This study attempts to incorporate the best of both worlds with flow disruption in the lower region (which is in contact with the heat source) and continued fluid mixing in the upper region of channel to enhance heat transfer. A better temperature distribution across the entire channel is achieved due to introduction of interacting channel phenomenon.
- Both kind of designs, the corrugated curved channel and interacting channels find their applications in specific conditions.
- Curved channels with corrugated base can be used in cases where we are more concerned with increasing convective heat transfer across channels and the pumping power is not the limiting factor.
- Interacting channels can be used in cases where the heat dissipation performance of MCHE is already sufficient with straight channels, however a decrease in overall

pumping power is required. It has the added benefit of providing a more uniform temperature distribution across the entire cooling area.

- Therefore, this interacting design is extremely useful in most practical cases where a uniform heat source is unlikely to be present. In all such cases, these connected channels provide a better overall channel performance.
- The passive mixing due to dean vortices improves the Nusselt number by a maximum of 20% at high Reynold numbers.
- The flow disruption in the lower region of channel can be introduced through the base corrugation of this channel, which further adds up to 4% improvement in overall convective heat transfer rates.
- The introduction of connecting bridge in parallel flow channel induces flow re-circulation within the bridge with only a marginal improvement in Nusselt number and pressure drop.
- For counter flow cases the local Nusselt number at bridge sees a major spike. While a decrease in pressure drop of up to a maximum of 30% was observed for interacting channels at 90° in counter flow condition.
- The expected mixing of fluid at channels with a bridge of 35° does not occur as per our requirement since the fluid velocity profile is not fully developed as it enters the curve therefore the dean vortices were not observed for this configuration. Therefore, the hybrid Curved-Interacting channel provides unsatisfactory results.
- The increase in aspect ratio provides an increase in Nusselt number, however this incremental increase diminishes at higher aspect ratio.
- For higher channel width the increase in height leads to smaller increase in Nusselt number.
- The nano-fluid relations developed by Rea et al. under predict the Nusselt number by 6% in comparison to the KKL model. Therefore we conclude that the results presented by Rea et al. are geometry dependent and not valid for general applications.

6.1 Future Scope:

- Multichannel models can be studied to determine the effect of plenum geometry and orientation of inlet upon the overall performance parameters.
- Multi-phase flow can be studied for both straight and curved channel models.
- Experimental study can be performed for the proposed model.

REFERENCES

[1] D. B. Tuckerman and R. F. W. Pease, "High-performance heat sinking for VLSI," *IEEE Electron Device Lett.*, vol. 2, no. 5, pp. 126–129, 1981, doi: 10.1109/EDL.1981.25367.

[2] S. S. Mehendafe, A. M. Jacobi, and R. K. Shah, "Fluid flow and heat transfer at micro- and meso-scales with application to heat exchanger design," *Appl. Mech. Rev.*, 2000, doi: 10.1115/1.3097347.

[3] S. G. Kandlikar, S. Garimella, D. Li, S. Colin, and M. King, *Heat Transfer and Fluid Flow in Minichannels and Microchannels*. 2014.

[4] N. T. Obot, "Toward a better understanding of friction and heat/mass transfer in microchannels - A literature review," *Microscale Thermophysical Engineering*. 2002, doi: 10.1080/10893950290053295.

[5] T. Bayraktar and S. B. Pidugu, "Characterization of liquid flows in microfluidic systems," *International Journal of Heat and Mass Transfer*. 2006, doi: 10.1016/j.ijheatmasstransfer.2005.11.007.

[6] M. Bahrami, M. M. Yovanovich, and J. R. Culham, "Pressure drop of fully-developed, laminar flow in rough microtubes," in *Proceedings of the 3rd International Conference on Microchannels and Minichannels, 2005*, 2005.

[7] M. Bahrami, M. M. Yovanovich, and J. R. Culham, "Pressure drop of fully-developed, laminar flow in microchannel of arbitrary cross-section," *J. Fluids Eng. Trans. ASME*, 2006, doi: 10.1115/1.2234786.

[8] S. I. Makino and H. Il Cheun, "Application of the real-time PCR for the detection of airborne microbial pathogens in reference to the anthrax spores," *Journal of Microbiological Methods*. 2003, doi: 10.1016/S0167-7012(03)00019-8.

[9] J. F. Regan *et al.*, "Environmental monitoring for biological threat agents using the autonomous pathogen detection system with multiplexed polymerase chain reaction," *Anal. Chem.*, 2008, doi: 10.1021/ac801125x.

[10] E. Moric-Janiszewska, L. Węglarz, and M. Szczurko, "Quantitative PCR as an alternative in the diagnosis of long-QT syndrome," *Biomed Res. Int.*, 2013, doi:

10.1155/2013/418604.

[11] B. Selva, J. Marchalot, and M. C. Jullien, “An optimized resistor pattern for temperature gradient control in microfluidics,” *J. Micromechanics Microengineering*, 2009, doi: 10.1088/0960-1317/19/6/065002.

[12] B. Selva, P. Mary, and M. C. Jullien, “Integration of a uniform and rapid heating source into microfluidic systems,” *Microfluid. Nanofluidics*, 2010, doi: 10.1007/s10404-009-0505-7.

[13] G. Gamrat, M. Favre-Marinet, and D. Asendrych, “Conduction and entrance effects on laminar liquid flow and heat transfer in rectangular microchannels,” *Int. J. Heat Mass Transf.*, 2005, doi: 10.1016/j.ijheatmasstransfer.2004.10.006.

[14] R. W. Knight, J. S. Goodling, D. J. Hall, and R. C. Jaeger, “Heat Sink Optimization with Application to Microchannels,” *IEEE Trans. Components, Hybrids, Manuf. Technol.*, 1992, doi: 10.1109/33.180049.

[15] P. S. Lee, S. V. Garimella, and D. Liu, “Investigation of heat transfer in rectangular microchannels,” *Int. J. Heat Mass Transf.*, 2005, doi: 10.1016/j.ijheatmasstransfer.2004.11.019.

[16] J. T. Liu, X. F. Peng, and W. M. Yan, “Numerical study of fluid flow and heat transfer in microchannel cooling passages,” *Int. J. Heat Mass Transf.*, 2007, doi: 10.1016/j.ijheatmasstransfer.2006.10.004.

[17] Y. Mishan, A. Mosyak, E. Pogrebnyak, and G. Hetsroni, “Effect of developing flow and thermal regime on momentum and heat transfer in micro-scale heat sink,” *Int. J. Heat Mass Transf.*, 2007, doi: 10.1016/j.ijheatmasstransfer.2006.12.003.

[18] J. Xu, Y. Song, W. Zhang, H. Zhang, and Y. Gan, “Numerical simulations of interrupted and conventional microchannel heat sinks,” *Int. J. Heat Mass Transf.*, 2008, doi: 10.1016/j.ijheatmasstransfer.2008.05.003.

[19] P. Rosa, T. G. Karayiannis, and M. W. Collins, “Single-phase heat transfer in microchannels: The importance of scaling effects,” *Applied Thermal Engineering*. 2009, doi: 10.1016/j.applthermaleng.2009.05.015.

[20] P. Hrnjak and X. Tu, “Single phase pressure drop in microchannels,” *Int. J. Heat Fluid*

Flow, 2007, doi: 10.1016/j.ijheatfluidflow.2006.05.005.

[21] T. M. Harms, M. J. Kazmierczak, and F. M. Gerner, "Developing convective heat transfer in deep rectangular microchannels," *Int. J. Heat Fluid Flow*, 1999, doi: 10.1016/S0142-727X(98)10055-3.

[22] T. Ahmad and I. Hassan, "Experimental analysis of microchannel entrance length characteristics using microparticle image velocimetry," *J. Fluids Eng. Trans. ASME*, 2010, doi: 10.1115/1.4001292.

[23] E. Galvis, S. Yarusevych, and J. R. Culham, "Incompressible laminar developing flow in microchannels," *J. Fluids Eng. Trans. ASME*, 2012, doi: 10.1115/1.4005736.

[24] H. R. Upadhye and S. G. Kandlikar, "Optimization of microchannel geometry for direct chip cooling using single phase heat transfer," in *Proceedings of the Second International Conference on Microchannels and Minichannels (ICMM2004)*, 2004.

[25] P. Gao, S. Le Person, and M. Favre-Marinet, "Scale effects on hydrodynamics and heat transfer in two-dimensional mini and microchannels," *Int. J. Therm. Sci.*, 2002, doi: 10.1016/S1290-0729(02)01389-3.

[26] R. K. Shah and A. L. London, *Laminar Flow Forced Convection in Ducts: A Source Book for Compact Heat Exchanger Analytical Data*. 1978.

[27] V. V. Dharaiya and S. G. Kandlikar, "Numerical investigation of heat transfer in rectangular microchannels under H2 boundary condition during developing and fully developed laminar flow," *J. Heat Transfer*, 2012, doi: 10.1115/1.4004934.

[28] M. K. Moharana and S. Khandekar, "Effect of aspect ratio of rectangular microchannels on the axial back conduction in its solid substrate," in *Progress in Microscale and Nanoscale Thermal and Fluid Sciences*, 2015.

[29] X. F. Peng and G. P. Peterson, "Convective heat transfer and flow friction for water flow in microchannel structures," *Int. J. Heat Mass Transf.*, 1996, doi: 10.1016/0017-9310(95)00327-4.

[30] A. M. Sahar, M. R. Özdemir, E. M. Fayyadh, J. Wissink, M. M. Mahmoud, and T. G. Karayiannis, "Single phase flow pressure drop and heat transfer in rectangular metallic microchannels," *Appl. Therm. Eng.*, 2016, doi: 10.1016/j.applthermaleng.2015.08.087.

[31] J. Zhang, Y. H. Diao, Y. H. Zhao, and Y. N. Zhang, "An experimental study of the characteristics of fluid flow and heat transfer in the multiport microchannel flat tube," *Appl. Therm. Eng.*, 2014, doi: 10.1016/j.applthermaleng.2014.01.008.

[32] A. G. Fedorov and R. Viskanta, "Three-dimensional conjugate heat transfer in the microchannel heat sink for electronic packaging," *Int. J. Heat Mass Transf.*, 2000, doi: 10.1016/S0017-9310(99)00151-9.

[33] G. Hetsroni, A. Mosyak, E. Pogrebnyak, and L. P. Yarin, "Fluid flow in micro-channels," *Int. J. Heat Mass Transf.*, 2005, doi: 10.1016/j.ijheatmasstransfer.2004.12.019.

[34] M. Renksizbulut and H. Niazmand, "Laminar flow and heat transfer in the entrance region of trapezoidal channels with constant wall temperature," *J. Heat Transfer*, 2006, doi: 10.1115/1.2130405.

[35] P. S. Lee and S. V. Garimella, "Thermally developing flow and heat transfer in rectangular microchannels of different aspect ratios," *Int. J. Heat Mass Transf.*, 2006, doi: 10.1016/j.ijheatmasstransfer.2006.02.011.

[36] A. N. Smith and H. Nochetto, "Laminar thermally developing flow in rectangular channels and parallel plates: uniform heat flux," *Heat Mass Transf. und Stoffuebertragung*, 2014, doi: 10.1007/s00231-014-1363-8.

[37] W. R. Dean and J. M. Hurst, "Note on the Motion of Fluid in a Curved Pipe," *Mathematika*, 1959, doi: 10.1112/S0025579300001947.

[38] W. R. Dean, " LXXII. The stream-line motion of fluid in a curved pipe (Second paper) ," *London, Edinburgh, Dublin Philos. Mag. J. Sci.*, 1928, doi: 10.1080/14786440408564513.

[39] A. P. Sudarsan and V. M. Ugaz, "Fluid mixing in planar spiral microchannels," *Lab Chip*, 2006, doi: 10.1039/b511524h.

[40] D. Di Carlo, "Inertial microfluidics," *Lab on a Chip*. 2009, doi: 10.1039/b912547g.

[41] J. L. Xu, Y. H. Gan, D. C. Zhang, and X. H. Li, "Microscale heat transfer enhancement using thermal boundary layer redeveloping concept," *Int. J. Heat Mass Transf.*, 2005, doi: 10.1016/j.ijheatmasstransfer.2004.12.008.

[42] J. A. Eastman, S. U. S. Choi, S. Li, W. Yu, and L. J. Thompson, "Anomalously increased

effective thermal conductivities of ethylene glycol-based nanofluids containing copper nanoparticles," *Appl. Phys. Lett.*, 2001, doi: 10.1063/1.1341218.

[43] S. U. S. Choi, S. Li, and J. A. Eastman, "Measuring thermal conductivity of fluids containing oxide nanoparticles," *J. Heat Transfer*, 1999, doi: 10.1115/1.2825978.

[44] S. K. Das, N. Putra, P. Thiesen, and W. Roetzel, "Temperature dependence of thermal conductivity enhancement for nanofluids," *J. Heat Transfer*, 2003, doi: 10.1115/1.1571080.

[45] U. Rea, T. McKrell, L. wen Hu, and J. Buongiorno, "Laminar convective heat transfer and viscous pressure loss of alumina-water and zirconia-water nanofluids," *Int. J. Heat Mass Transf.*, 2009, doi: 10.1016/j.ijheatmasstransfer.2008.10.025.

[46] S. R. Hosseini, M. Sheikholeslami, M. Ghasemian, and D. D. Ganji, "Nanofluid heat transfer analysis in a microchannel heat sink (MCHS) under the effect of magnetic field by means of KKL model," *Powder Technol.*, 2018, doi: 10.1016/j.powtec.2017.10.043.

[47] W. Peiyi and W. A. Little, "Measurement of friction factors for the flow of gases in very fine channels used for microminiature Joule-Thomson refrigerators," *Cryogenics (Guildf).*, 1983, doi: 10.1016/0011-2275(83)90150-9.

[48] W. Wagner and A. Kruse, *Properties of Water and Steam / Zustandsgrößen von Wasser und Wasserdampf*. 1998.

[49] R. D. Blevins, "Applied fluid dynamics handbook.," 1984, doi: 10.1016/0894-1777(94)90012-4.

[50] A. Bejan, *Convection Heat Transfer: Fourth Edition*. 2013.

[51] F. White, "Chapter 6 Viscous Flow in Ducts," *Fluid Mech. Seventh Ed.*, 2011.

[52] R. L. Hamilton, "Thermal conductivity of heterogeneous two-component systems," *Ind. Eng. Chem. Fundam.*, 1962, doi: 10.1021/i160003a005.

[53] J. Li and C. Kleinstreuer, "Thermal performance of nanofluid flow in microchannels," *Int. J. Heat Fluid Flow*, 2008, doi: 10.1016/j.ijheatfluidflow.2008.01.005.

[54] H. C. Brinkman, "The viscosity of concentrated suspensions and solutions," *J. Chem. Phys.*, 1952, doi: 10.1063/1.1700493.

[55] J. Q. Yong and C. J. Teo, “Mixing and heat transfer enhancement in microchannels containing converging-diverging passages,” *J. Heat Transfer*, 2014, doi: 10.1115/1.4026090.

[56] S. Harikrishnan and S. Tiwari, “Heat transfer characteristics of sinusoidal wavy channel with secondary corrugations,” *Int. J. Therm. Sci.*, 2019, doi: 10.1016/j.ijthermalsci.2019.105973.